Cellular and Molecular Neurobiology (2025) 45:91
https://doi.org/10.1007/s10571-025-01615-4

ORIGINAL RESEARCH

Neuroprotective Effects of the Nonsteroidal Anti-inflammatory Drug Celecoxib Against Caspase-1-dependent Pyroptosis Partially by Suppressing the HMGB1/TLR4 Pathway

Yu Sun[1,2] · Shucai Jiang[3] · Yan Feng[4] · Lei Chen[5] · Zhe Feng[1,2] · Caibin Gao[6] · Weifang Rong[7] · Feng Wang[8]

Received: 2 June 2025 / Accepted: 27 September 2025

Abstract

This study evaluated the protective effects of celecoxib on epilepsy and explore its potential involvement in regulating pyroptosis and the high mobility group box 1 (HMGB1)/Toll-like receptor 4 (TLR4) signaling pathway. Adult male Sprague–Dawley rats were injected with ferrous chloride ($FeCl_2$) with or without celecoxib for 7 consecutive days. After sacrifice, tissues were collected for neurological function assessments, magnetic resonance imaging, and multiple tissue analyses. Intracerebral injection of $FeCl_2$ in rats induced severe seizures, microglial recruitment and polarization, ferroptosis, pyroptosis, and inflammation in the frontal cortex. In the hippocampus, $FeCl_2$ injection led to neuronal loss, reduced synaptic complexity, and aberrant HMGB1 expression. Celecoxib treatment delayed seizure onset and significantly reduced the severity and duration of seizures, the extent of injury, and neurological impairments caused by $FeCl_2$ exposure. These effects were mediated through the suppression of HMGB1/TLR4 signaling and inhibition of key pro-inflammatory cytokines. Celecoxib treatment mitigated neuronal loss, improved synaptic complexity, stabilized microglial activity, inhibited astrocyte proliferation, and modulated HMGB1 expression. In conclusion, celecoxib effectively attenuated $FeCl_2$-induced inflammation and neural injury partially by inhibiting the HMGB1/TLR4 pathway, thereby suppressing pyroptosis and reactive gliosis. These effects improved seizure, highlighting the therapeutic potential of celecoxib for managing epilepsy following hemorrhagic brain injury.

✉ Weifang Rong
weifangrong@hotmail.com

✉ Feng Wang
nxwwang@zju.edu.cn

1 School of Basic Medical Science, Ningxia Medical University, Yinchuan 750000, China

2 Ningxia Key Laboratory of Cerebrocranial Disease, Incubation Base of National Key Laboratory, Ningxia Medical University, Yinchuan 750000, China

3 Weifang People's Hospital, Weifang 261044, China

4 RWTH Aachen University, 52074 Aachen, Germany

5 Department of Neurosurgery, The First People's Hospital of Shizuishan, Shizuishan 753200, China

6 General Hospital of Ningxia Medical University, Yinchuan 750003, China

7 Shanghai Jiao Tong University College of Basic Medical Sciences, Shanghai 200025, China

8 Department of Neurosurgery, The First Affiliated Hospital of Zhejiang University, Hangzhou 310000, China

Published online: 23 October 2025

Graphical Abstract

Title: Molecular pathological mechanisms of acute brain injury involving brain parenchymal and vascular damage

Legend: Intracranial hemorrhage activates PAMPs and PRPs, whereas iron ions promote ROS accumulation, resulting in the downregulation of GSH and GPX4, ultimately inducing ferroptosis. HMGB1, released in response to brain parenchymal damage. binds to TLR4, triggering a robust inflammatory cascade that contributes to pyroptosis and neuroinflammation.

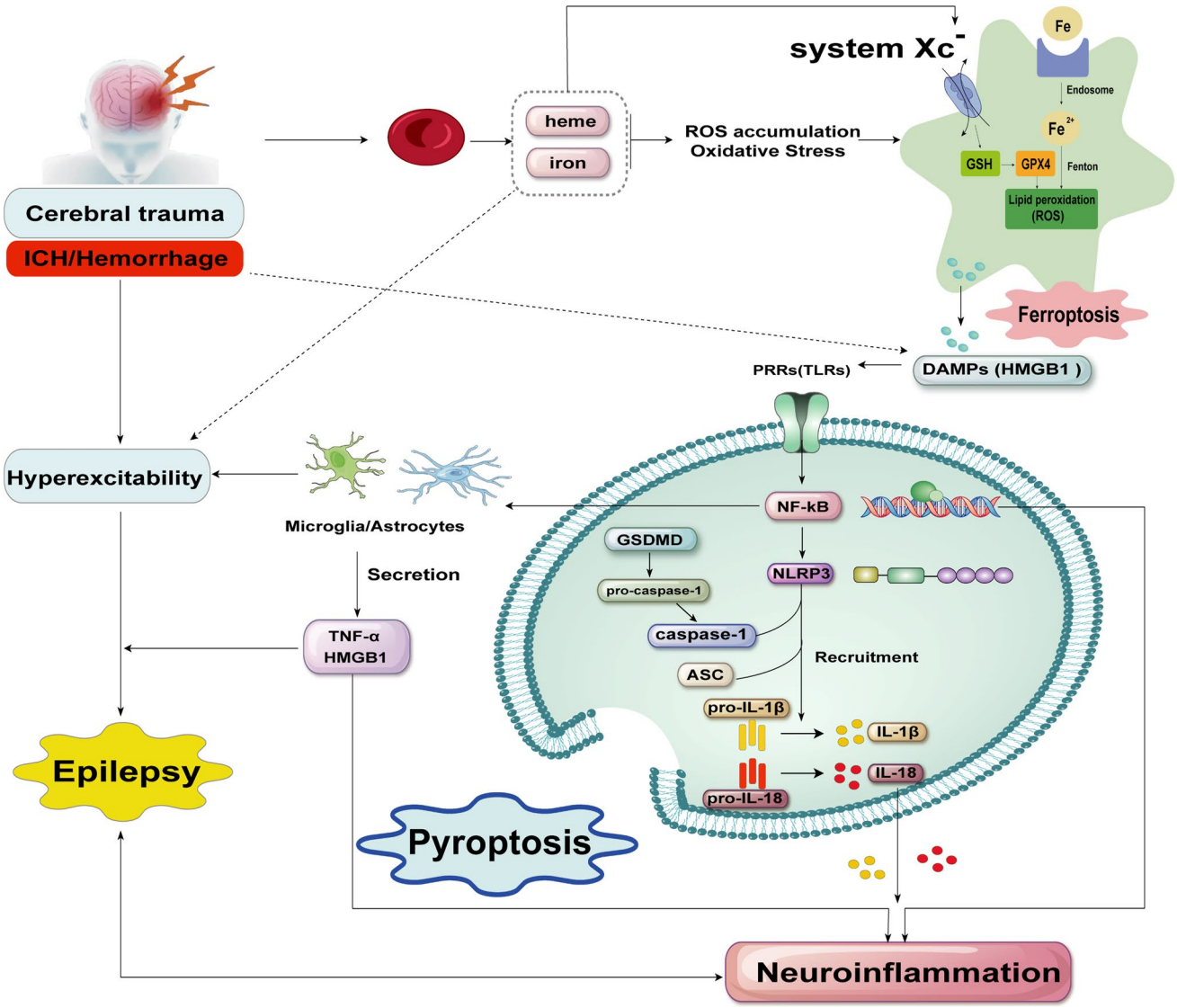

Keywords Epilepsy · Neuroinflammation · HMGB1 · TLR4 · Pyroptosis · Celecoxib

Introduction

Epilepsy is a neurological disease caused by multiple factors, with intracerebral hemorrhage (ICH) and traumatic brain injury (TBI) being the major causes of acquired epilepsy (Maas et al. 2008; Thijs et al. 2019). Key inflammatory mediators are highly expressed in the brain during epilepsy, and they can potentially affect neuronal function and excitability. Inflammation was found to enhance seizure susceptibility in both preclinical and clinical models (Vezzani et al. 2011). Cyclooxygenase-2 (COX-2), an enzyme involved in the synthesis of the pro-inflammatory mediator prostaglandin, plays a critical role in brain inflammation (Morgan et al. 2020), and it has emerged as a potential target for epilepsy treatment (Dedeurwaerdere et al. 2012). Celecoxib (CCX), a nonsteroidal sulfonamide anti-inflammatory drug that selectively inhibits COX-2

(Puljak et al. 2017), has demonstrated efficacy in alleviating neuroinflammation (van Vliet et al. 2018) and lowering susceptibility to various types of chronic epilepsies (Rawat et al. 2019; Zhou et al. 2018). Iron accumulation and iron-induced neurotoxicity are common features of both ICH and TBI (Conrad et al. 2021). The degradation of hemoglobin results in heme release, leading to excessive Fe^{2+} accumulation. Iron overload triggers oxidative lipid damage, resulting in neuronal death via apoptosis, pyroptosis, and ferroptosis (Hirano et al. 2019; Qureshi et al. 2009). Cellular damage and inflammation contribute to the onset and propagation of epilepsy (Vezzani et al. 2008). However, the role of COX-2 in iron-induced epilepsy and the effect of CCX on epilepsy following acute ICH or TBI remain unclear.

Ferroptosis is a recently identified form of programmed cell death that occurs in the early stages of hemorrhagic injury, and it is associated with multiple secondary injuries (Chen et al. 2021; Yan et al. 2021). It is primarily driven by the depletion of intracellular glutathione (GSH) and subsequent inactivation of glutathione peroxidase 4 (GPX4) (Jiang et al. 2021). Ferroptotic cells release damage-related molecular patterns (DAMPs), which initiate other forms of programmed cell death (Frank and Vince 2019). Pyroptosis is another type of programmed cell death that induces inflammation (Shi et al. 2017), and it is widely involved in the progression of several organ diseases (Loveless et al. 2021). It is triggered when pattern recognition receptors (PRRs) recognize DAMPs, leading to the formation and activation of inflammasomes (Burdette et al. 2021). There are two pyroptosis pathways, namely the classical caspase-1 pathway and the nonclassical pathway that activates caspase-4, caspase-5, and caspase-11 (Frank and Vince 2019). Inflammation-mediated pyroptosis activates the NLRP3 inflammasome through DAMPs, resulting in activation of the classical caspase-1 pathway (Hsu et al. 2021). Subsequently, the activation of gasdermin D (GSDMD) and release of inflammatory factors, such as interleukin (IL)-1β and IL-18, contribute to pathological progression after ICH and the development of epilepsy (Atabaki et al. 2023; Corps et al. 2015; Tanaka et al. 2023). Whether CCX can affect ferroptosis and pyroptosis warrants further investigation.

High mobility group box 1 (HMGB1) is an alarmin protein that acts through several receptors, such as PRRs and receptor for advanced glycation end-products, to mediate inflammation and immune responses (Tang et al. 2023). It participates in the inflammatory cascade through both passive release from dying cells and active secretion from immune cells (Tang et al. 2023). In the intercellular space, HMGB1 binds to Toll-like receptor 4 (TLR4) on glial cells, inducing glial activation and proliferation, exacerbating inflammation, and ultimately promoting multiple forms of cell death (Banks et al. 2023). Numerous studies have reported the essential role of HMGB1/TLR4 signaling in inflammation following brain injury (Andersson et al. 2018a, 2018b; Kamaşak et al. 2020; Ping et al. 2021; Ravizza et al. 2018; Sun et al. 2020; Tian et al. 2020). In experimental models of epilepsy and brain injury, activation of the HMGB1/TLR4 pathway promoted the onset of epilepsy by triggering tissue damage and inflammatory responses (Paudel et al. 2019). In the brain tissues and peripheral blood of patients with epilepsy, both HMGB1 and TLR4 are upregulated, highlighting their potential as epileptic seizure biomarkers (Yang et al. 2017). Moreover, a recent study confirmed that ferroptotic cells release high levels of DAMPs, primarily HMGB1 (Wen et al. 2019). Thus, investigating the role of HMGB1 in the pathogenesis of epilepsy might provide insights into the complex interplay among hemorrhage, injury, and epilepsy.

Based on this information, we hypothesized that CCX protects against seizures and neurological dysfunction following hemorrhagic brain injury by inhibiting glial activation, neuroinflammation, and pyroptosis through suppression of the HMGB1/TLR4 pathway. This hypothesis was tested using a rat model of $FeCl_2$-induced epilepsy.

Materials and Methods

Animals and Grouping

Adult male Sprague–Dawley (SD) rats weighing 220 ± 30 g were obtained from the Experimental Animal Center of Ningxia Medical University (Yinchuan, China). The study protocol was approved by the Medical Ethics Committee of Ningxia Medical University and performed in accordance with the guidelines for animal use and care issued by the Science and Technology Ministry of China. All measures were taken to minimize the suffering of the animals.

Rats were housed under a 12-h/12-h light/dark cycle and standard laboratory conditions, including room temperature of 23 ± 1 °C and ad libitum access to food and water. After 1 week of acclimation, animals were randomized into one of three groups: sham surgery (sham group), $FeCl_2$ injection model ($FeCl_2$ group), and $FeCl_2$ + CCX (CCX group). CCX (catalog number: 169590–42-5; MedChemExpress, Monmouth Junction, NJ, USA) was prepared as a suspension in saline and administered via the esophagus (20 mg/kg) 1 h after $FeCl_2$ injection, followed by daily doses for 7 consecutive days. At the end of the experiment, rats were euthanized, and brain tissues surrounding the injection sites were collected and stored at − 80 °C for further experiments.

$FeCl_2$ Injection Model

Following anesthetization with isoflurane and stereotaxic placement, a burr hole was drilled into the skull of each SD rat at a predetermined coordinate. $FeCl_2$ (catalog number: 45093, Sigma-Aldrich, St. Louis, MO, USA; 5 µL of 0.2 mol/L $FeCl_2$ in saline) was injected stereotactically over 5 min using a micro-syringe (Gaoge, Dongguan, China, 0–10 µL) into the right motor cortex (area M1; coordinates: anteroposterior, − 3.0 mm; lateral, 2.0 mm; and ventral, 2.0 mm). The needle remained in place for an additional 10 min post-injection to prevent reflux. Cortical electroencephalography was performed using stainless steel screw electrodes (coordinates: anteroposterior, − 6.0 mm; lateral, − 4.0 mm), with a reference electrode placed in the cerebellar region (coordinates: anteroposterior, − 7.0 mm; lateral, 0 mm). Rats in the sham group received injections of saline solution. The ipsilateral hemisphere (right side) was used for all subsequent morphological analyses and western blotting (WB).

Rats were allowed to recover for 20 min after surgery. Successful modeling was determined by a seizure score of 4 or higher as assessed by the Racine scale. The scale is graded as follows (Lüttjohann et al. 2009): 0 = no abnormality; 1 = staring; 2 = head nodding or wet-dog shaking, with or without facial tics; 3 = unilateral forelimb clonus; 4 = bilateral forelimb clonus with continuous head nodding; and 5 = severe bilateral forelimb clonus with loss of balance, falling, or generalized tonic–clonic seizures. Latency to epileptic seizure onset and daily seizure severity were recorded for 7 consecutive days.

Neurological Function Tests

Neurological deficits were assessed using the modified Garcia scoring system, a neurobehavioral test used to quantify neurological dysfunction. This system evaluates six categories: spontaneous activity, limb movement symmetry, forepaw outstretching, climbing ability, body proprioception, and vibrissae response. Each category was scored from 0 (worst) to 3 (best), with the total score ranging from 0 to 18.

Motor recovery was evaluated by the Terzis grooming test (TGT). Approximately 5 mL of water were sprayed on the nose and mouth of each rat using a syringe to induce grooming behavior in both upper limbs. The grooming response was rated according to the highest reach of the contralateral forelimb as follows: class 0, no response in the upper limb; class 1, elbow flexion below the nose; class 2, reaching the nose; class 3, below the eye; class 4, reaching the eye; and class 5, reaching the ear or higher.

Muscle strength was measured by the grip strength test. Rats grasped a grid connected to a grip strength meter with each forelimb separately, and each forelimb's grip strength was recorded three times. The average grip strength per forelimb was then calculated. The values before and after the intervention were compared to assess motor function changes. All measurements were conducted by the same examiner to minimize bias.

Magnetic Resonance Imaging (MRI)

Imaging was performed using a SIGNA Architect 3.0 T superconducting MRI scanner (GE Healthcare, Chicago, IL, USA) equipped with an eight-channel dedicated small animal coil (Shanghai Chengguang Medical Technology Co., Ltd., Shanghai, China). Following anesthesia with isoflurane, rats were placed in a prone position with their heads centered within the coil, permitting spontaneous breathing. T1-weighted imaging was performed with a spin-echo sequence using a repetition time of 470 ms and an echo time of 10 ms. T2-weighted imaging was performed with a fast spin-echo sequence using a repetition time of 2500 ms and an echo time of 85 ms. Scans were acquired in the coronal plane, obtaining 12 slices, each with a thickness of 2 mm and an interslice gap of 0.2 mm. The resolution matrix was 128×128, and the field of view was 80×80 mm^2. Imaging analysis was performed using the ADW 4.7 workstation (GE Healthcare) and processed using READY VIEW software. Injury areas in the right frontal lobe were measured at different time points. All measurements were independently performed by two experienced physicians, and the average values were recorded.

Histopathological Analysis

For Nissl staining, tissue sections were immersed in Nissl staining solution (catalog number: C0117; Beyotime, Haimen, China) for 5 min, washed with double-distilled water, and mounted with Permount. Images were captured under a microscope (Nikon, Tokyo, Japan).

Hematoxylin–eosin (H&E) staining was performed using a commercial kit (Beyotime) following the manufacturer's protocol.

For Golgi staining, fresh rat brain tissues were immersed in solutions A and B for 2 weeks, followed by solution C for 3 days. Sections were cut at a thickness of 100 µm using a vibratome (Leica, Wetzlar, Germany), washed with double-distilled water for 8 min, and dehydrated in a graded ethanol series (50%, 75%, 95%, and 100%) for 16 min. Finally, the sections were sealed with neutral gum and imaged at × 200 and × 1000 magnification using an Eclipse Ci-L microscope. Analysis was performed using Image-Pro Plus 6.0 software.

For Perls staining, paraffin-embedded sections were treated sequentially with xylene I and xylene II for 8 min each, followed by a graded ethanol series (absolute ethanol I, absolute ethanol II, 90% ethanol, 80% ethanol, and 70% ethanol for 5 min each). Next, the sections were washed with

deionized water and incubated in Perls solution (1:1 ratio of Perls A and B solutions) for 20 min.

ImmunoFluorescence (IF)

The heart of each rat was perfused transcardially with 4% paraformaldehyde, after which the brain tissue was removed and post-fixed with 4% paraformaldehyde. The tissue was then dehydrated in a sucrose gradient for 48 h and sectioned coronally after freezing. Sections were washed, blocked with 5% bovine serum albumin for 30 min, and then incubated overnight at 4 °C with the following primary antibodies (all from Abcam, Cambridge, UK): ionized calcium-binding adapter molecule 1 [Iba-1 (1:200)], glial fibrillary acidic protein [GFAP (1:200)], HMGB1 (1:300), and TLR4 (1:200). After PBS washes, sections were incubated for 1 h at room temperature with the secondary antibody Alexa Fluor 647 (1:500, goat anti-rabbit, Abcam). Subsequently, sections were counterstained with 4′,6′-diamino-2-phenylindole (DAPI, Invitrogen, Waltham, MA, USA) for 5 min before imaging on a fluorescence microscope (Nikon). Digital images around regions of interest were randomly captured for each section. The cell count and fluorescence intensity were quantified using ImageJ software (US National Institutes of Health, Bethesda, MD, USA).

Transmission Electron Microscopy (TEM)

The frontal cortex of each rat's brain was surgically removed and immediately fixed in glutaraldehyde. Subsequently, samples were post-fixed with osmium tetroxide, dehydrated in a graded ethanol series, and embedded in epoxy resin for ultrastructural analysis. Ultrathin sections (approximately 50–70 nm thick) were then prepared using an ultramicrotome, followed by staining with uranyl acetate and lead citrate for visualization via TEM. The stained sections were examined at an accelerating voltage of 80 kV, and digital images were captured for analysis.

WB

The cortex of each rat brain was carefully micro-dissected from euthanized animals and immediately frozen in liquid nitrogen. The tissue samples were then homogenized and lysed in RIPA buffer supplemented with a protease inhibitor mixture for WB. Equal amounts of protein (8 μg) were loaded into each lane for 8% SDS–PAGE and transferred to 0.22-μm polyvinylidene fluoride membranes preactivated with methanol (MilliporeSigma, Burlington, MA, USA). The membranes were blocked with 5% nonfat milk, incubated in Tris-buffered saline with Tween-20 at room temperature for 2 h, and then stained with specific primary antibodies at 4 °C overnight against HMGB1 (1:1000, Abcam), TLR4 (1:400, Abmart, China), GFAP (1:1000, Abcam), Iba-1 (1:1000, Abcam), GSDMD (1:1000, Abcam), cleaved caspase-1 (1:1000, Affinity, China), GPX4 (1:1000, Abcam), xCT (1:500, Affinity), and glyceraldehyde 3-phosphate dehydrogenase (GAPDH; 1:1000, Affinity), with β-actin (1:1000, Affinity) serving as an internal control. After primary antibody incubation, the membranes were washed and incubated for 1 h with the secondary antibody IRDye 700w (1:5000, goat anti-rabbit, LI-COR, Lincoln, NE, USA). Band intensities were quantified using Image Lab software (Bio-Rad), with target protein signals normalized to those of GAPDH or β-actin.

Fluorescence Quantitative Reverse Transcription PCR (RT-qPCR)

Total mRNA was isolated from hippocampal tissues using an RNA kit (TIANGEN, Beijing, China), and the concentration and purity of RNA were determined using a Nanodrop 2000C spectrophotometer. The extracted RNA was reverse-transcribed into cDNA using a reverse transcription kit (TaKaRa, Shiga, Japan). SYBR green-based RT-qPCR was conducted on a CFX96 PCR system (Bio-Rad, Hercules, CA, USA) to quantify the mRNA expression of target genes, with β-actin serving as an internal control. Primers were synthesized by Shanghai Sangon Biotech Co., Ltd. (Shanghai, China), and their sequences were as follows:

HMGB1 forward, 5′-AAGGCTGACAAGGCTCGTTATG-3′; HMGB1 reverse, 5′-GGCGGTACTCAGAACAGAACAAG-3′;

TLR4 forward, 5′-GAATGAGGACTGGGTGAGAAATGAG-3′; TLR4 reverse, 5′-TGGATGATGTTGGCAGCAATGG-3′;

β-actin forward, 5′-ACTGCCGCATCCTCTTCCTC-3′; and β-actin reverse, 5′-AACCGCTCGTTGCCAATAGTG-3′.

The reaction protocol consisted of 40 cycles of 95 °C for 30 s and 60 °C for 30 s. The Ct values were obtained, and the relative expression of target genes was calculated using the $2^{-\Delta\Delta Ct}$ method.

Enzyme-Linked Immunosorbent Assay (ELISA)

The levels of IL-1β, IL-18, nuclear factor kappa B, NLRP3, HMGB1, TLR4, and ASC were measured using ELISA kits (JONLNBIO, Shanghai, China) according to the manufacturer's instructions.

TUNEL Staining

Antigen-retrieved brain sections were incubated with a TUNEL reaction mixture (catalog number: C1089, Beyotime) for 1 h at room temperature. Following 20-min PBS

washes, the slides were counterstained with DAPI for 5 min. The sections were then washed twice with PBS and observed under an inverted fluorescence microscope. TUNEL-positive cells were quantified by ImageJ software. The apoptosis index was calculated as the ratio of TUNEL-positive cells to DAPI-stained nuclei.

Caspase-1 Activity Assay

Activated caspase-1 levels were assessed using a colorimetric assay kit (Beyotime). Briefly, damaged cortical tissues were lysed in ice-cold RIPA buffer containing 1 mM phenylmethylsulfonyl fluoride and centrifuged at 2000 × *g* at 4 ℃ for 10 min. The supernatant was collected and incubated with 2 mM acetyl-Tyr-Val-Al-Asp-nitroaniline at 37 ℃ for 2 h. Caspase-1 activity was quantified by measuring peptide nucleic acid release at 405 nm using an M2 microplate reader (Molecular Devices, San Jose, CA, USA). Activity levels were normalized to total protein, which was measured by the Bradford method.

Gene Ontology (GO) Functional Enrichment Analysis

The Comparative Toxicogenomics Database (CTD) was used to identify gene targets associated with epilepsy, injury, inflammation, hemorrhage, and pyroptosis. An intersection analysis of these genes was conducted and visualized using the VennDiagram package in R. The intersection targets were then uploaded to the STRING database, and the resulting file was imported into Cytoscape 3.9.0 software to build a protein–protein interaction (PPI) network and screen core target genes. The CTD Set Analyzer platform was used for GO functional enrichment analysis of the intersection targets and hub genes. The results were visualized using the ggplot2 and ggrepel packages in R.

Molecular Docking

Molecular docking was conducted using AutoDock 4.2 software to assess the binding affinity of CCX for HMGB1. Human HMGB1 X-ray crystal structures (PDB code: 2LY4) were obtained from the Protein Data Bank to complete the docking simulation. The resulting conformations and binding energies were saved to a molecular database file, and the ligand–protein complexes were visualized using PyMOL. The interplay between HMGB1 and CCX was detected using ZDOCK and RDOCK, which are common tools for detailed protein–protein docking prediction.

Statistical Analysis

Data are presented as the mean ± standard deviation based on at least three independent experiments. ELISA results were analyzed by two-way analysis of variance (ANOVA) followed by Bonferroni's post hoc multiple comparisons test. Other datasets were compared by one-way ANOVA followed by least significant difference post hoc analysis or Student's *t*-test. Statistical significance was set at $p < 0.05$.

All analyses were conducted under a triple-blind design: tissue samples were randomly coded and provided to analysts, measurements followed a standardized operating procedure, and statisticians performed analyses using only coded datasets without group identifiers. No outliers were identified in the dataset.

Results

CCX prolongs Seizure Latency and Reduces the Severity and Duration Of Seizures Induced by $FeCl_2$ Injection

Previous studies utilized $FeCl_2$ at doses of 0.2–0.4 mol/L (Chen et al. 2022a; Das et al. 2017; Willmore and Rubin 1982; Willmore et al. 1978a, 1978b). To determine the optimal dose for our model, we administered stereotactic injections of 0.2 (3, 5, or 10 µL) and 0.4 mol/L (5 or 10 µL) $FeCl_2$ into the frontal cortex in each rat. As presented in Table 1, the injection of both 3 and 5 µL of 0.2 mol/L $FeCl_2$ resulted in 0% mortality (six animals/group), indicating stable model survival.

Comparing seizure severity in the two groups (Table 2), the 3-µL group had an initial Racine seizure score lower than 4 (3.5 ± 0.5, six animals/group), which progressively decreased to less than 2 (1.7 ± 0.8, six animals/group) by day 7 (Fig. 1A). The 5-µL group had a Racine seizure score

Table 1 Effects of different doses of $FeCl_2$ on male SD rats

Treatment	Dose (µL)	Seizure (n)			Death (n)	Mortality (%)
		Stage 3	Stage 4	Stage 5		
0.4 mol/L $FeCl_2$	10	0	0	6	5	83.3
0.4 mol/L $FeCl_2$	5	0	1	5	3	50
0.2 mol/L $FeCl_2$	10	0	0	6	2	33.3
0.2 mol/L $FeCl_2$	5	0	2	4	0	0
0.2 mol/L $FeCl_2$	3	2	3	1	0	0

Table 2 Daily maximum Racine seizure scores in each group

Time (days)	Saline	0.2 mol/L $FeCl_2$ (3 μL)	0.2 mol/L $FeCl_2$ (5 μL)	CCX + 0.2 mol/L $FeCl_2$ (5 μL)
1	0	3.5 ± 0.5	4.4 ± 0.5	3.8 ± 0.9
2	0	3.3 ± 0.5	3.7 ± 0.5	3.4 ± 0.5
3	0	2.5 ± 0.5	3.4 ± 0.8	3.0 ± 0.6
4	0	2.7 ± 0.8	3.5 ± 0.5	2.5 ± 0.5
5	0	2.8 ± 0.4	3.4 ± 0.5	2.4 ± 0.5
6	0	1.8 ± 0.4	3.1 ± 0.4	2.1 ± 0.7
7	0	1.7 ± 0.8	2.9 ± 0.3	1.8 ± 0.7

exceeding 4 (4.4 ± 0.5, eight animals/group) on day 7, with most rats reaching a score of 3 (2.9 ± 0.3, eight animals/group). Furthermore, the epileptic seizure duration was significantly longer in the 5-μL group than in the 3-μL group (Fig. 1B), although seizure latency was not significantly different between the two groups (Fig. 1C). Based on these results, we identified 5 μL and 0.2 mol/L as the optimal injection volume and dose, respectively.

On the day of surgery, rats in the CCX group had a significantly lower average maximum Racine seizure score than those in the $FeCl_2$ group (3.8 ± 0.9 *vs.* 4.4 ± 0.5, eight animals/group; Fig. 1D). Additionally, the duration of seizures with Racine scores higher than 4 was significantly shorter in the CCX group (Fig. 1E), and seizure onset was delayed (Fig. 1F). Epilepsy scores were significantly reduced in the CCX group from day 4 to day 7 post-surgery (Fig. 1D). By day 7, the average Racine seizure score in the CCX group was lower than 2 (1.8 ± 0.7, eight animals/group). These results suggest that CCX treatment significantly reduced seizure scores, delayed seizure onset, and shortened seizure duration in rats injected with $FeCl_2$.

Improves Neurological Function Following $FeCl_2$ Exposure

To investigate the protective effect of CCX, we evaluated sensory and motor function recovery using the 18-point Garcia test before (0 h) and after $FeCl_2$ injection (12, 24, 36, 48, 60, and 72 h). The average score in the sham group was 18, indicating intact motor function (Fig. 2C). Rats in the $FeCl_2$ group exhibited the greatest motor function impairment at 24 h post-injection, with gradual improvement afterward. By 36 h, the CCX group displayed significant motor function recovery, with a Garcia score greater than 10 points (Table 3), which was notably higher than that in the $FeCl_2$ group (eight animals/group). There was no significant difference in the average scores in the $FeCl_2$ group at 60 and 72 h, indicating that motor recovery plateaued, with the average score being lower than 11 at 72 h. By contrast, continued improvement was noted in the CCX group, with the average score at 72 h exceeding 14, which was significantly higher than that in the $FeCl_2$ group (eight animals/group).

To determine the location of neuromotor dysfunction, the TGT (Fig. 2A) was performed to evaluate bilateral forelimb motor function and grip strength in the rats (Fig. 2B). At 12 h, 1 day, and 3 days post-surgery, rats in the $FeCl_2$ group demonstrated marked muscle weakness in the contralateral (left) limbs and paws, with the lowest average value

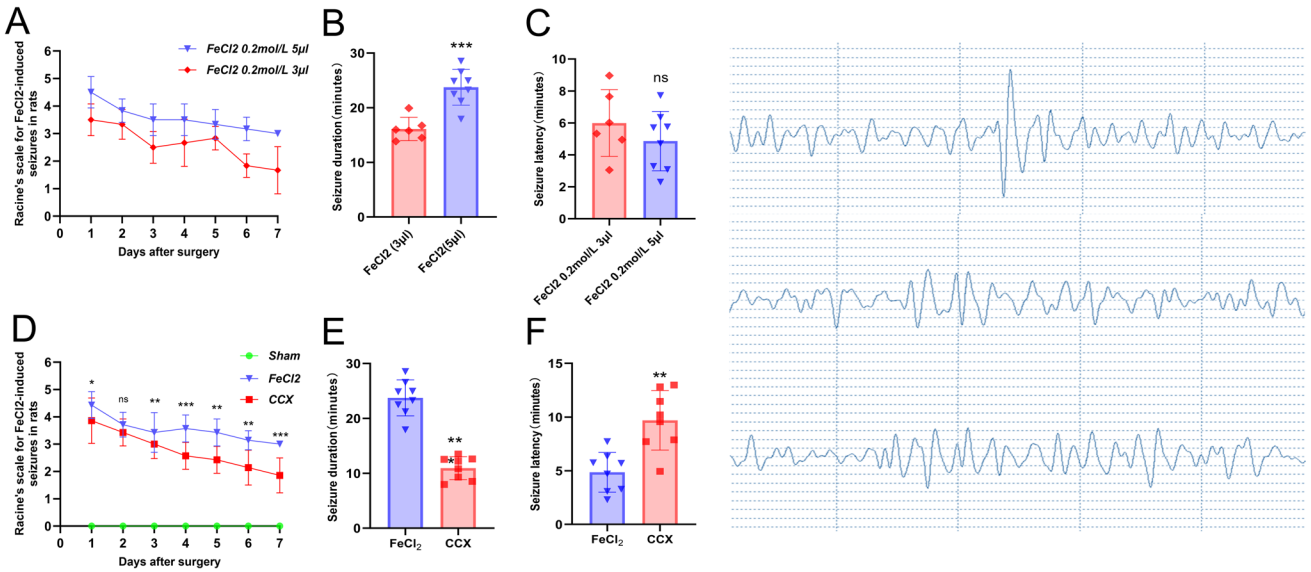

Fig. 1 Seizure scores, duration, and latency following $FeCl_2$ injection. **A–C** Daily maximum Racine scores, seizure duration, and latency (min) following the administration of different doses of $FeCl_2$. **D–F** Effects of CCX on Racine scores, seizure duration, and seizure latency (min) in the $FeCl_2$-induced seizure model. ***$p < 0.001$, **$p < 0.01$, *$p < 0.05$

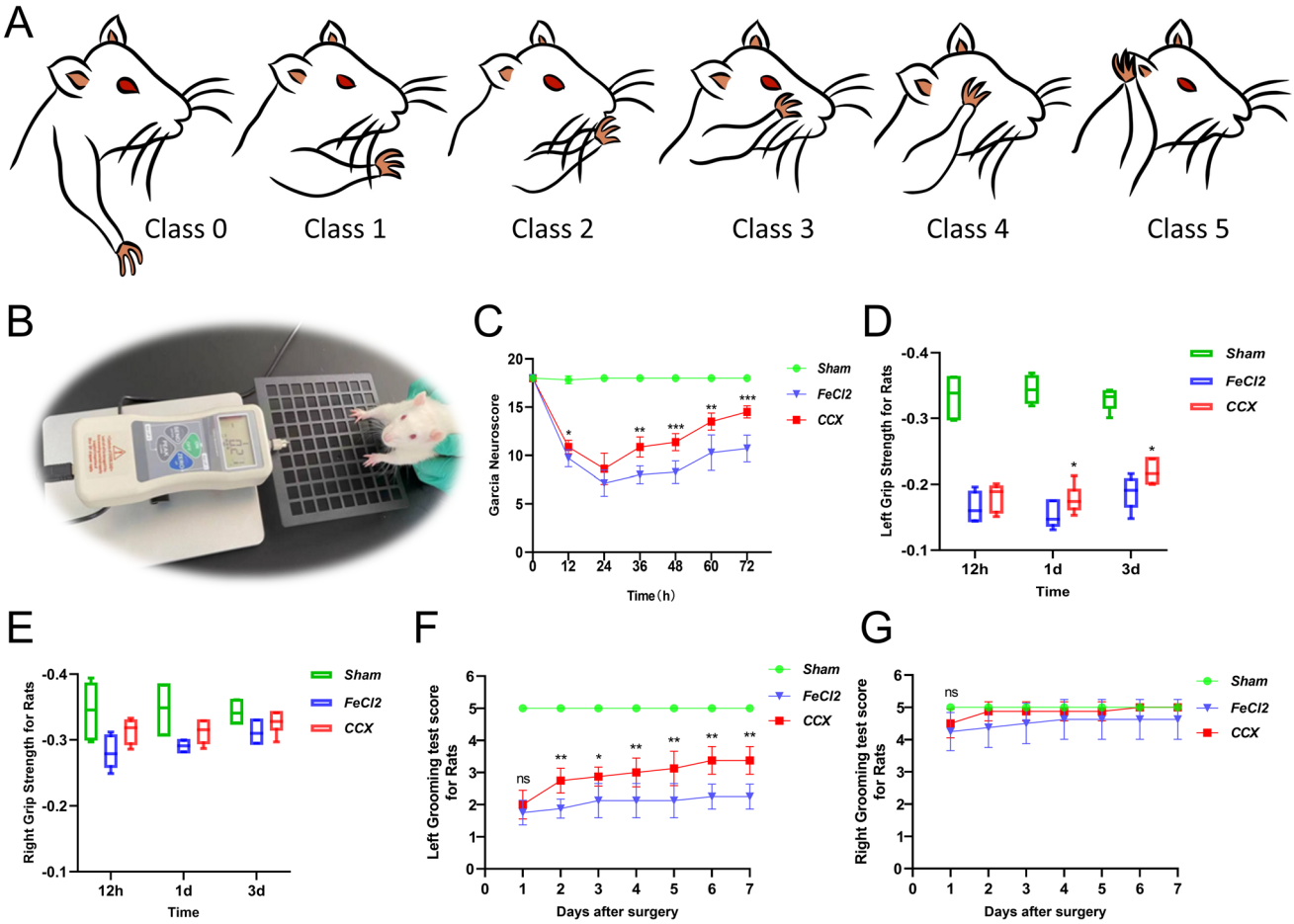

Fig. 2 Neurofunctional impairment analysis. **A** Schematic of the TGT. **B** Grip strength test. **C** Motor function evaluation using the 18-point Garcia test over 72 h post-surgery. **D–E** Measurement of contralateral (left) and ipsilateral (right) forelimb grip strength within 3 days post-surgery using the grip strength test. **F–G** Average TGT scores in different groups within 1 week post-surgery. ***$p < 0.001$, **$p < 0.01$, *$p < 0.05$

Table 3 Garcia scores within 72 h post-injection

Time	0 h	12 h	24 h	36 h	48 h	60 h	72 h
Sham	18.00 ± 0.00	18.00 ± 0.00	18.00 ± 0.00	18.00 ± 0.00	18.00 ± 0.00	18.00 ± 0.00	18.00 ± 0.00
$FeCl_2$	18.00 ± 0.00	9.71 ± 0.95	7.14 ± 1.46	8.00 ± 1.00	8.29 ± 1.25	10.29 ± 1.98	10.71 ± 1.50
CCX	18.00 ± 0.00	10.88 ± 0.83	8.63 ± 1.92	10.88 ± 1.25	11.38 ± 1.06	13.50 ± 1.07	14.50 ± 0.76

observed on day 1, compared with the findings in the sham group (n = eight animals/group; Fig. 2D, F). This pattern aligned with the Garcia test results. Rats in the CCX group did not exhibit significant improvement in forelimb muscle strength at 12 h post-surgery (Fig. 2F). However, notable recovery of grip strength was observed at 1 and 3 days post-surgery (eight animals/group; Fig. 2F). Motor deficits on the contralateral side were alleviated at 2 days post-surgery (eight animals/group, Fig. 2F). On the ipsilateral (right) side, no significant difference was observed in TGT results compared with those in the Sham group, excluding day 1 (eight animals/group; Fig. 2G). No significant difference in grip strength was found on the ipsilateral side at any time point (Fig. 2E). These findings suggested that $FeCl_2$ injection-induced damage predominantly affected the contralateral (left) side. Treatment with CCX significantly improved neurological dysfunction induced by $FeCl_2$ injection.

CCX Reduces the Cortical Injury Area in Rats After $FeCl_2$ Injection

We further explored whether $FeCl_2$-induced tissue damage is related to iron overload. In full-brain images (fresh and perfused) of $FeCl_2$-injected rats, extensive

hemosiderin deposition was observed across the brain. Compared with the findings in the $FeCl_2$ group, rats in the CCX group displayed a markedly reduced injury area. To further confirm the protective effect of CCX, an MRI was performed on days 3 and 7 post-injection to quantify cortical injury in $FeCl_2$-injected rats. Four coronal levels (bregma − 3.96, 0.00, 1.08, and 2.08) associated with the $FeCl_2$ injection site were examined (Fig. 3A). On day 3 post-injection, the injured area displayed low signal intensity on both T1- and T2-weighted imaging, with an injury level of 3 (Fig. 3B, C). The average injury area in the CCX group was significantly smaller than that in the $FeCl_2$ group (1.77 ± 0.55 mm^2 *vs.* 3.83 ± 0.52 mm^2; Fig. 3F). On day 7 post-injection, the injury had expanded, as illustrated by an increased area at level 3 in both the $FeCl_2$ and CCX groups (7.46 ± 0.56 and 5.70 ± 0.49 mm^2, respectively; Fig. 3D, E). The injury also extended to level 2 in these groups (4.74 ± 0.46 and

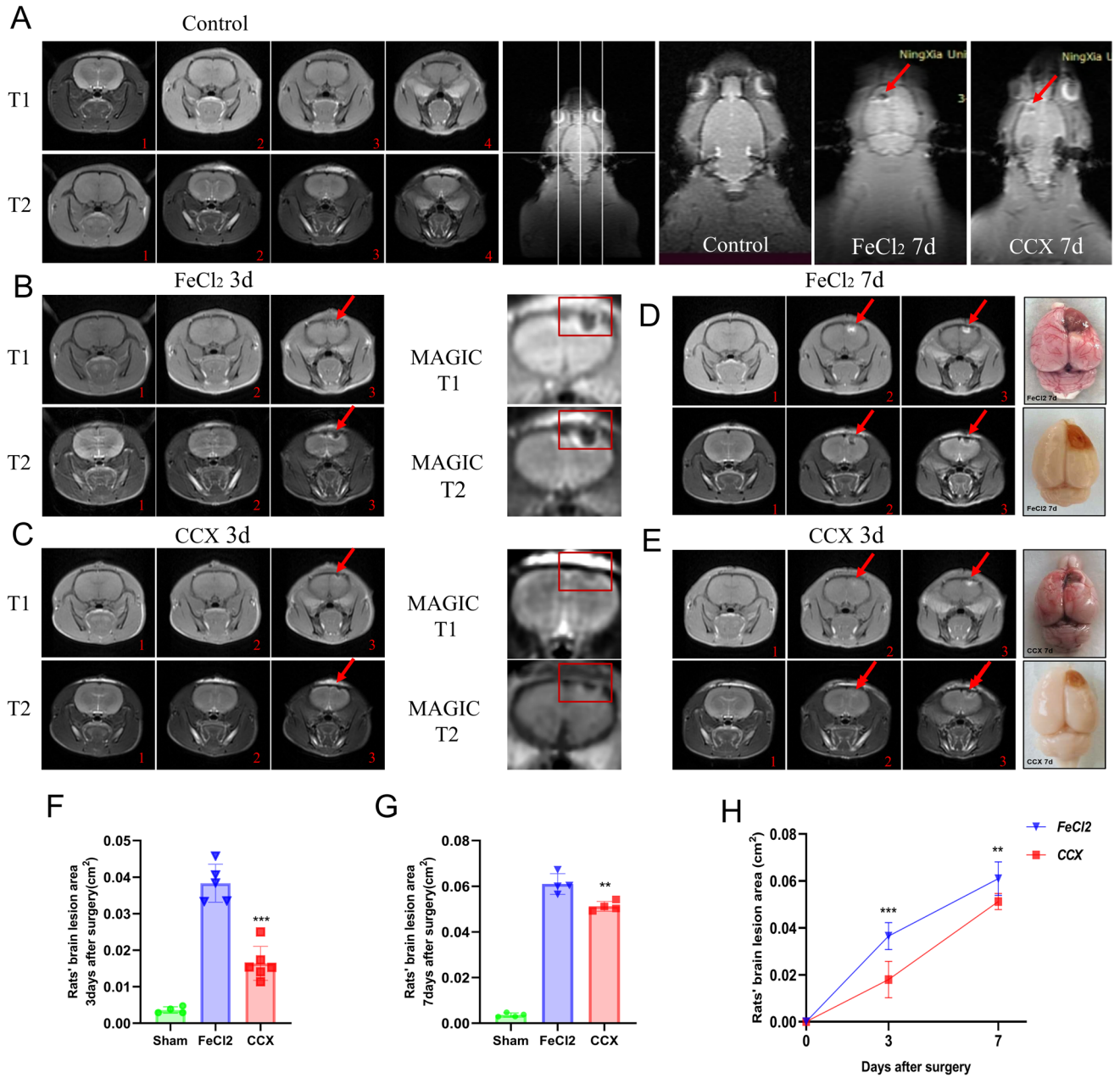

Fig. 3 MRI of brain injury. **A** T1- and T2-weighted brain imaging of rats in the control and treatment groups. **B–C** MR images of rats in the $FeCl_2$ and CCX groups at 3 days post-surgery. **D–E** MR images of rats in the $FeCl_2$ and CCX groups at 7 days post-surgery. **F–G** Quantification of the injury area over time in all groups. **H** Progression of the injury area in the $FeCl_2$ and CCX groups. $^{***}p < 0.001$, $^{**}p < 0.01$

4.55 ± 0.33 mm^2 respectively; Fig. 3D, E). This progression indicates that $FeCl_2$-induced injury is dynamic and progressive over time. However, when averaging the injury areas at levels 2 and 3, the overall injury area was significantly smaller in the CCX group than in the $FeCl_2$ group on day 7 post-injection (Fig. 3G). Collectively, CCX treatment effectively reduced the cortical injury area at both 3 and 7 days after $FeCl_2$ injection, decelerating the progression of injury (Fig. 3H).

CCX Alleviates Hemosiderin-Induced Cell Loss, Cellular Damage, Synaptic Alterations, and Iron Accumulation

To investigate the specific impact of $FeCl_2$-induced brain injury, we first validated the injection site. Figure 4A presents the injection site at 24 h post-surgery, confirming the accurate injection of $FeCl_2$ into the motor cortex (area M1). At day 7 post-surgery, Nissl staining and H&E staining were performed in both the frontal cortex and CA1 hippocampal region. Nissl staining (Fig. 4B) revealed significant cell loss, swelling, and deformation in the frontal cortex in the $FeCl_2$

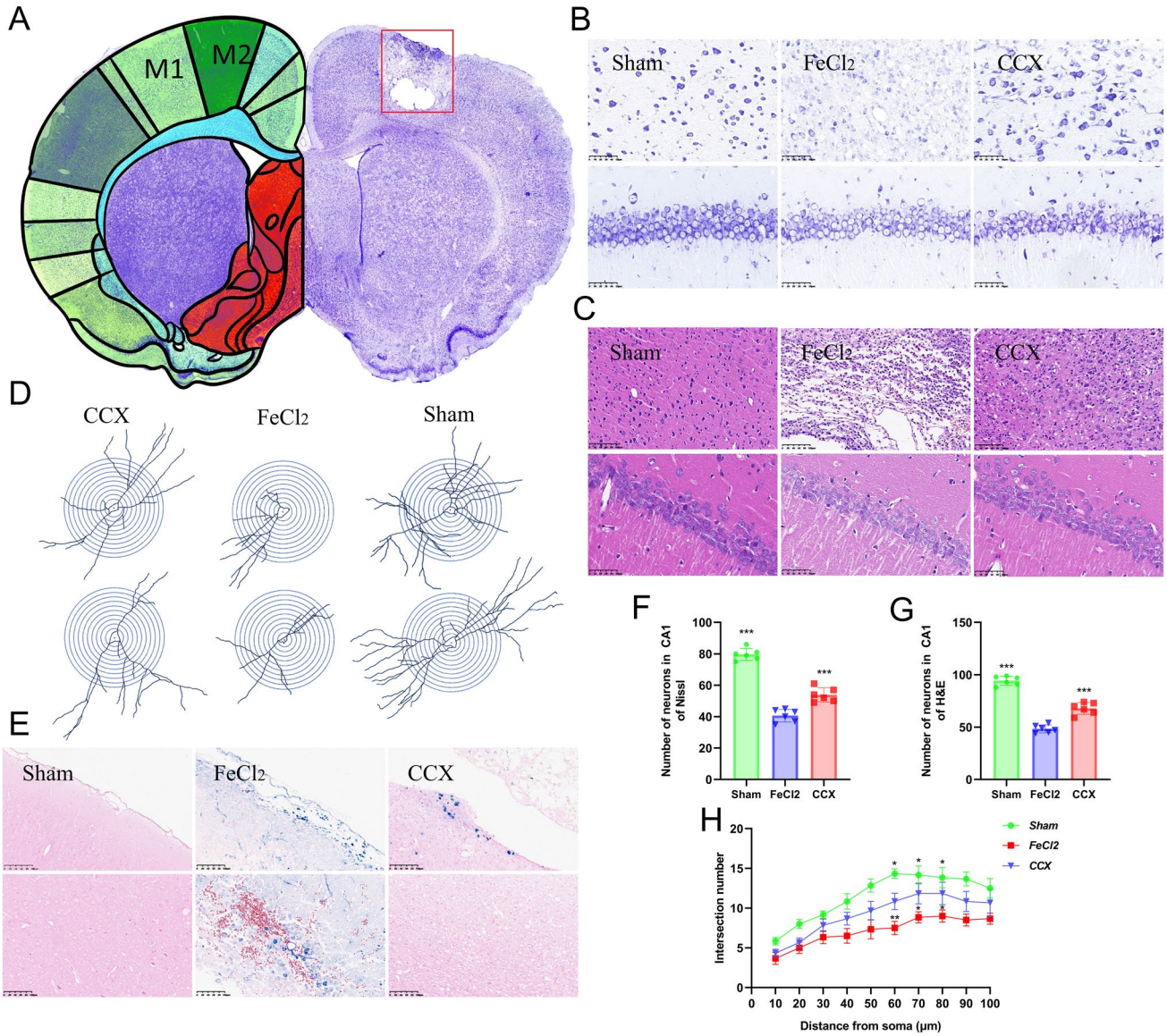

Fig. 4 Morphological injury in rat brain tissues. **A** Injection site verification at 24 h post-surgery. **B** Nissl staining of the frontal cortex and CA1 hippocampal region. **C** H&E staining of the frontal cortex and CA1 hippocampal region. **D** Sholl analysis of neuronal morphology in the hippocampus. **E** Perls iron staining of the frontal cortex. **F** Neuron counts in CA1 using Nissl staining. **G** Neuron counts in CA1 using H&E staining. **H** Dendritic intersection analysis of hippocampal neurons. ***$p < 0.001$, **$p < 0.01$, *$p < 0.05$

group, indicating severe neuronal damage compared with that in the sham group. These changes were notably mitigated by CCX treatment. Similar patterns were observed in the CA1 hippocampal region (Fig. 4B). Neuron counts were significantly lower in the $FeCl_2$ group than in the sham group (six animals/group; Fig. 4F), whereas CCX treatment significantly preserved neuronal populations in CA1 after $FeCl_2$ injection (six animals/group; Fig. 4F). Consistently, H&E staining demonstrated that compared with the findings in sham-treated rats, $FeCl_2$-treated rats exhibited increased cell death, cytoplasmic condensation, nuclear shrinkage or dissolution, enlarged intercellular spaces, and disordered cellular arrangement in the frontal cortex. In the CCX group, cell death was reduced, and fewer cells exhibited cytoplasmic swelling and degeneration (six animals/group; Fig. 4G). We also analyzed neuronal morphology using Golgi staining. The number of pyramidal neurons with dendritic extensions reaching 60–80 μm from the soma significantly decreased after $FeCl_2$ injection, (three animals/group; Fig. 4E, I), whereas CCX administration improved dendritic complexity (three animals/group; Fig. 4E, I).

$FeCl_2$ injection can mimic severe cellular damage caused by acute hemorrhage (Caliaperumal et al. 2012). Perls iron staining confirmed hemosiderin deposits and increased positive cell counts at the edge and center of the injury area, accompanied by red blood cell clots in intercellular spaces, in $FeCl_2$-injected rats (Fig. 4E). CCX-treated rats displayed a significant reduction in positively stained cells, with improved cellular morphology and quantity relative to the findings in the $FeCl_2$ group (three animals/group; Fig. 4I). These findings suggested that CCX can reduce injury and mitigate epilepsy development by inhibiting the recruitment and phagocytosis of acute-phase immune cells, thereby preventing hemosiderin accumulation at the injury site.

CCX Inhibits Glial Cell Activation and Proliferation

$FeCl_2$ injection activated microglia, which migrated toward the damaged cortical area (Fig. 5A). In the $FeCl_2$ group, cortical microglia exhibited an ameboid or round morphology, indicating an activated state, with significantly increased cell counts compared with those in the sham group (Fig. 5B). CCX treatment reduced the proportion of activated microglia in the cortical region (Fig. 5D) and inhibited their proliferation (Fig. 5E). Notably, although the hippocampus was not directly injured, microglial recruitment was observed in the CA1 hippocampal region (Fig. 5C). In $FeCl_2$-injected rats, hippocampal microglia migrated towards the cortex, displaying a bipolar morphology at the hippocampus–cortex boundary but becoming rounded upon reaching the cortex (Fig. 5C). CCX treatment reduced both the number of activated microglia and the extent of migration toward the hippocampus–cortex boundary (data not shown). Unlike microglia, hippocampal astrocytes mainly exhibited proliferative characteristics (Fig. 6A). Analysis of astrocyte proliferation revealed increased fluorescence intensity in the DG, CA1, and CA3 regions after $FeCl_2$ injection, with the most substantial increase observed in the DG region. CCX treatment effectively inhibited astrocyte proliferation in these areas (Fig. 6B–D). WB revealed elevated expression of Iba-1 (microglia marker) and GFAP (astrocyte marker) in the frontal cortex and hippocampus after $FeCl_2$ injection, indicating local glial proliferation. CCX treatment markedly downregulated these markers (Fig. 6E–G), suggesting that glial cell activation plays a key role in the development of $FeCl_2$-induced seizures and cortical damage. CCX effectively inhibited glial cell activation, recruitment, and proliferation, thereby reducing glial cell-mediated inflammatory responses following $FeCl_2$ injection.

CCX Reduces Inflammation and Caspase-1–Mediated Pyroptosis

To determine whether $FeCl_2$ injection induces inflammation, we measured the levels of inflammatory factors, including HMGB1, TLR4, nuclear factor kappa B, NLRP3, IL-18, and IL-1β, in the rat frontal cortex 24 h post-injury using ELISA. Although the levels of these factors were changed in the $FeCl_2$ group compared with those in sham-operated animals, the differences were not significant. Extending the observation period to 7 days post-surgery, we observed significantly increased concentrations of these inflammatory factors in both the frontal cortex and hippocampus in the $FeCl_2$ group, whereas their levels were notably reduced by CCX treatment (Fig. 7A–F). These findings suggested that cell death drives inflammation, leading to the upregulation of inflammatory factors after $FeCl_2$ injection.

To further elucidate the role of cell death in this process, we assessed apoptosis in the frontal cortex using TUNEL staining 1 week after $FeCl_2$ injection (Fig. 8A). The percentage of dead cells was significantly higher in the $FeCl_2$ group than in the sham group, whereas that in the CA1 hippocampal region did not significantly differ between the two groups (Fig. 8B, C). CCX treatment markedly reduced cell death in the frontal cortex (Fig. 8B). Subsequent TEM of the frontal cortex revealed the type of cell death. After $FeCl_2$ injection, cells underwent pyroptosis, characterized by cytoplasmic swelling, cell membrane disruption, and the formation of bubble-like protrusions surrounding the cell membrane, known as pyroptotic bodies (indicated by arrows in Fig. 8F). Molecular analyses supported these findings, illustrating that $FeCl_2$ injection expression the levels of proteins associated with the classical pyroptosis pathway, including cleaved caspase-1, GSDMD, and ASC (Fig. 8E, H, I), accompanied by increased caspase-1 activity (Fig. 8D). CCX treatment

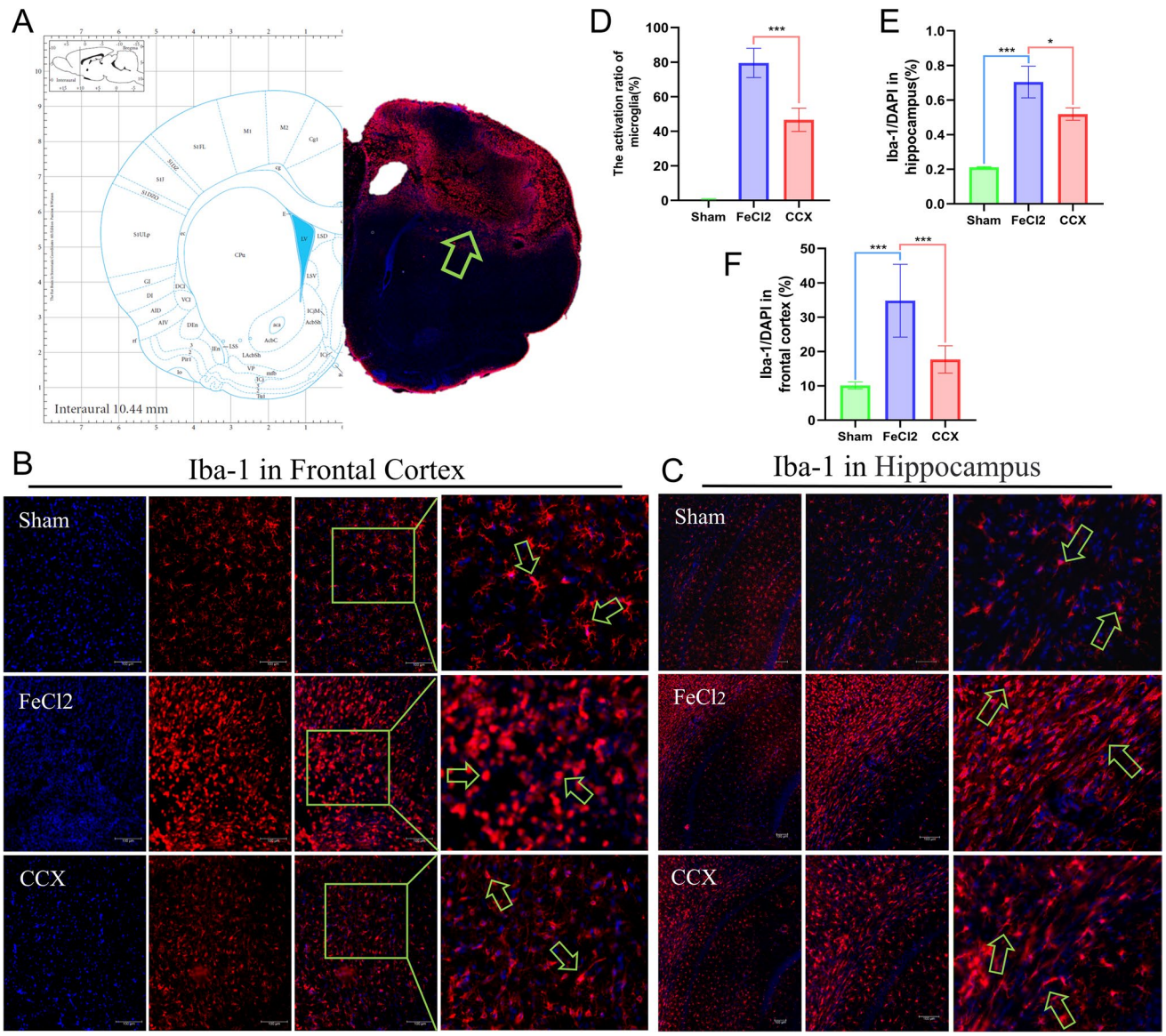

Fig. 5 Regulatory effect of CCX on microglia. **A** Migration of microglia toward the injured site. **B** IF staining of microglia in the frontal cortex. **C** Quantification of microglia in the frontal cortex. **D** Quantification of activated microglia in the frontal cortex. **E** Microglial recruitment in the hippocampus at 7 days post-surgery. **F** IF staining of microglia in the hippocampus. **G** Quantification of microglia in the hippocampus. $^{***}p < 0.001$, $^{**}p < 0.01$, $^{*}p < 0.05$

significantly suppressed cleaved caspase-1, GSDMD, and ASC expression (Fig. 8E, H, I) and decreased caspase-1 activity (Fig. 8D) in $FeCl_2$-injected rats.

Furthermore, TEM revealed features of ferroptosis, including membrane disruption, cell bubbling, and mitochondrial shrinkage (indicated by arrows in Fig. 8J). $FeCl_2$ injection also led to significant reductions in the expression of the ferroptosis-related proteins xCT and GPX4 (Fig. 8L, M), lowered GSH levels (Fig. 8N), and increased MDA levels (Fig. 8O). However, CCX treatment did not significantly affect xCT or GPX4 expression and GSH or MDA levels (Fig. 8L–O).

Overall, after $FeCl_2$ administration, significant pyroptosis and ferroptosis were observed in the cortex, along with the increased production of inflammatory factors. CCX inhibited pyroptosis and downregulated pyroptosis-associated inflammatory factors, but it had limited effects on ferroptosis-related proteins such as GPX4 and xCT.

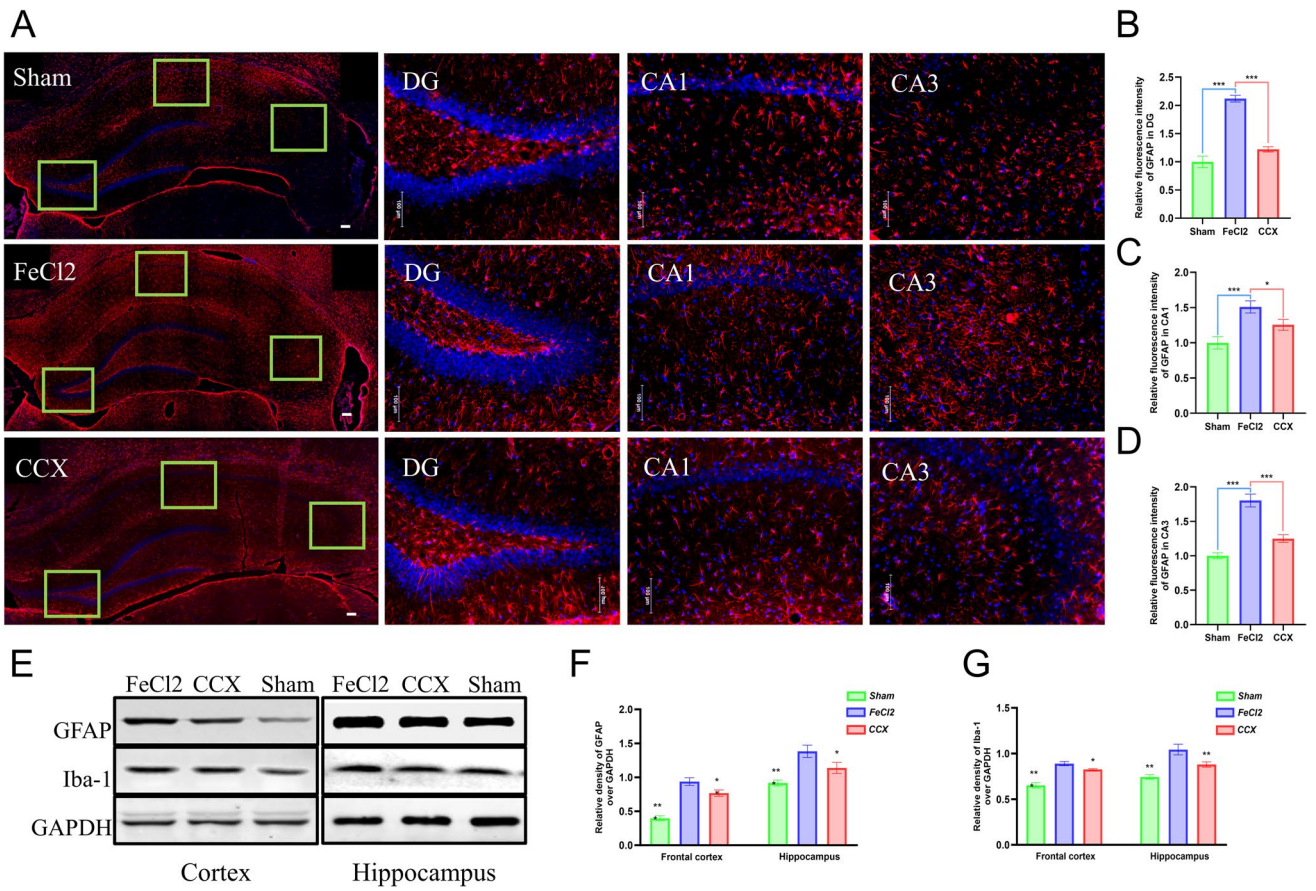

Fig. 6 Regulatory effect of CCX on astrocytes. **A** IF staining of astrocytes in different hippocampal regions. **B–D** Quantification of GFAP intensity in the DG, CA1, and CA3 regions. **E** WB of GFAP and Iba-1. **F–G** Relative protein expression of GFAP and Iba-1. $^{***}p < 0.001$, $^{**}p < 0.01$, $^{*}p < 0.05$

CCX Regulates Inflammatory Responses and Pyroptosis Induced by $FeCl_2$ Injection Via *the HMGB1/TLR4 Axis*

Next, we used the CTD database to identify genes implicated in epilepsy, injury, inflammation, hemorrhage, and pyroptosis. By intersecting these categories, we generated a gene list that included HMGB1 and TLR4 (Fig. 9A). This selection yielded 46 relevant genes, which we used to construct a PPI network. Notably, HMGB1 appeared in an upstream node in this network (Fig. 9B), indicating its involvement in various disease-related processes, including pyroptosis. Subsequently, GO enrichment analysis was performed on this set of genes using the Hipplot platform. The analysis identified 11 significantly enriched GO terms, including five in molecular function, one in cellular components, and five in biological processes (Fig. 9C). Several interactive genes were associated with pyroptosis, with the main enriched biological processes being pyroptosis, defense response to bacteria, and regulation of the innate immune response (Fig. 9D). These results indicated that HMGB1, as a key factor inducing inflammation, was involved in multiple injury-related processes, such as epilepsy, injury, inflammation, hemorrhage, and pyroptosis. Subsequently, molecular docking studies were performed using AutoDock Vina software. The result revealed a binding energy of − 5 kcal/mol between CCX and HMGB1 (Fig. 9E), suggesting that CCX can bind directly to HMGB1 to exert its therapeutic effect.

To further confirm that CCX inhibited pyroptosis via the HMGB1/TLR4 pathway, we analyzed the expression of HMGB1 and TLR4 in the frontal cortex using WB and IF staining (Fig. 10A–G). IF staining revealed a significant increase in HMGB1 and TLR4 expression in the $FeCl_2$-injured cortex compared with that in sham-operated rats, whereas CCX treatment reduced this upregulation (Fig. 10C, D). The WB results demonstrated similar trends (three animals/group; Fig. 10F, G). RT-qPCR further validated these findings at the transcriptional level (three animals/group; Fig. 10H, I). Interestingly, we observed region-specific differences in HMGB1 expression in the hippocampus. In the ipsilateral (right) hippocampus, HMGB1 expression was significantly lower in the $FeCl_2$ group than in the sham group (three animals/

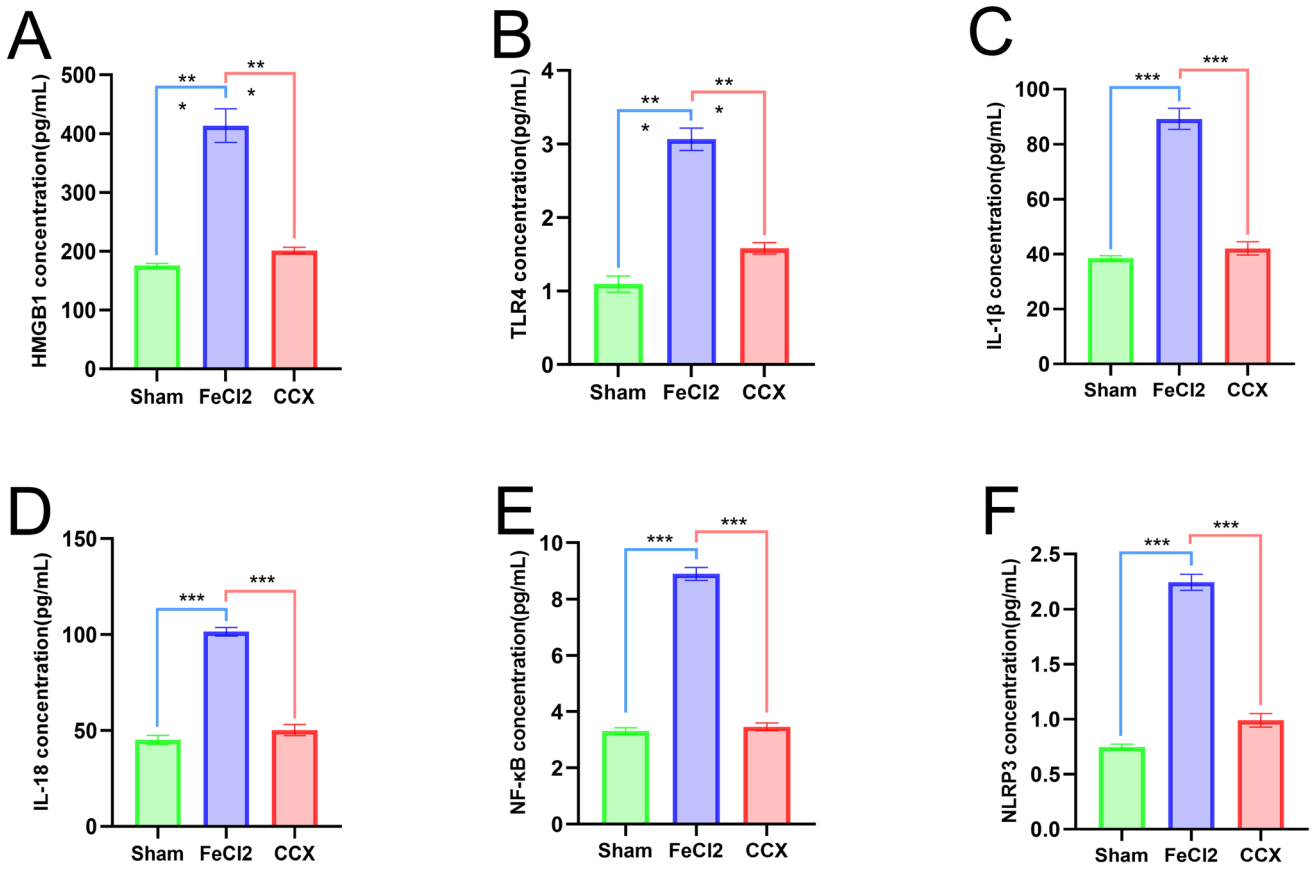

Fig. 7 Inflammatory cytokine expression. **A–F** ELISA of inflammatory cytokine levels at 7 days post-surgery. ***$p < 0.001$, **$p < 0.01$, *$p < 0.05$

group; Fig. 10J). Although CCX treatment elevated HMGB1 expression (three animals/group; Fig. 10K), its expression remained lower than that in the sham group (three animals/group; Fig. 10K). Conversely, in the contralateral hippocampus (left), $FeCl_2$ injection led to a significant increase in HMGB1 expression relative to that in the sham group (three animals/group; Fig. 10K), and CCX treatment effectively mitigated this increase (three animals/group; Fig. 10K). However, TLR4 expression did not change in either hippocampal region (three animals/group; Fig. 10L). The differential expression of HMGB1 in the hippocampus might be related to microglial behavior following $FeCl_2$ injection. Taken together, CCX regulates pyroptosis and inflammation progression via the HMGB1/TLR4 pathway in the frontal cortex, exerting neuroprotective effects after intracerebral hemorrhage.

Discussion

Iron-induced epilepsy is a well-established model resembling human post-traumatic epilepsy that was initially proposed by Willmore et al. (Willmore et al. 1978b). In this model, iron compounds, such as $FeCl_3$ or $FeCl_2$, are injected into the somatosensory cortex to mimic the release of iron from hemoglobin following brain injury (Willmore et al. 1978a). Excessive iron ions induce cell membrane structural damage through the Fenton reaction, leading to cell death (Jiang et al. 2021). Because of its stability, high seizure incidence, and relatively simple pathogenesis, the iron-induced epilepsy model is commonly used in studies of epilepsy following hemorrhagic brain injury (Das et al. 2017; Keith and Huang 2019; Komatsu et al. 2000; Prakash et al. 2019, 2021). The $FeCl_2$ dose has varied across studies, possibly because of differences in animal strains, age, and anesthetic methods. In our study, isoflurane was used as the anesthetic, as chloral hydrate has inhibitory effects on seizures (Fong et al. 2017), which could interfere with Racine score evaluations. Isoflurane, as an inhalation anesthetic, offers a short duration of action and rapid recovery. After assessing both mortality and seizure severity, we determined that, under isoflurane anesthesia, a dose of 0.2 mol/L $FeCl_2$ in a volume of 5 µL should be used to establish a stable epileptic model in 4–6-week-old SD rats.

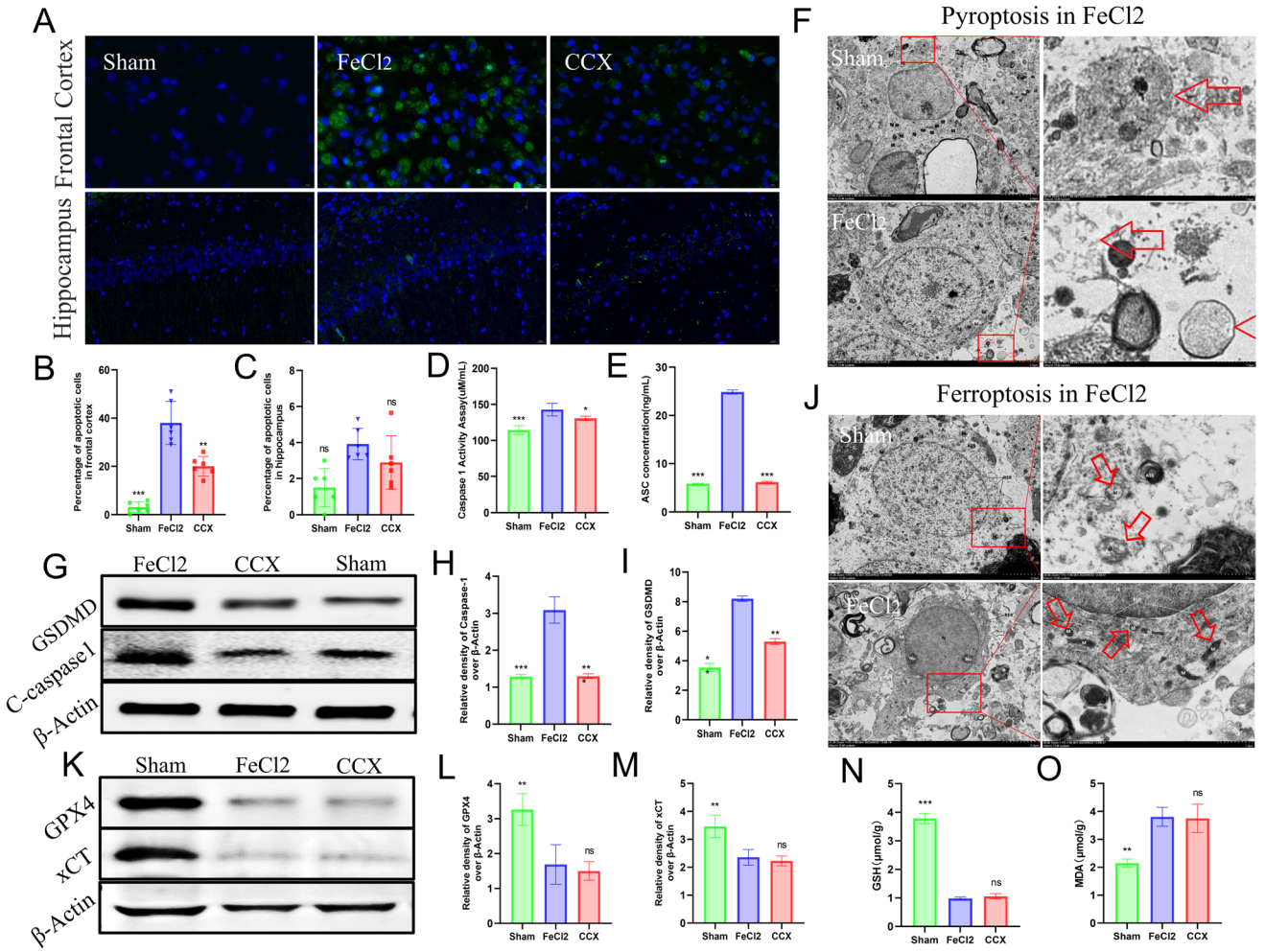

Fig. 8 Assessment of cell death. **A** TUNEL staining of the frontal cortex and CA1 hippocampal region. **B–C** Percentage of apoptotic cells in the frontal cortex and hippocampus. **D** Caspase-1 activity (μM/mL). **E** ASC concentrations. **F** Representative images reveal pyroptosis. **G** WB of GSDMD and cleaved caspase-1. **H–I** Relative protein expression of GSDMD and cleaved caspase-1. **J** Representative ferroptosis images. **K** WB of xCT and GPX4. **L–M** Relative protein expression of xCT and GPX4. **N** GSH levels (μmol/g). (O) MDA concentrations (μmol/g). $^{***}p < 0.001$, $^{**}p < 0.01$, $^{*}p < 0.05$

Early seizure onset following brain injury is associated with the development of acute trauma (Wang et al. 2020). In addition to severe epileptic seizures, we also observed neurological dysfunction, including somatosensory and motor impairments, in model rats attributable to $FeCl_2$-induced damage to the motor cortex. Severe epileptic seizures and clinical sensorimotor impairments have been reported in models of TBI and spinal cord injury (Huang et al. 2022; Wu et al. 2019). Furthermore, the severity of seizure activity is positively correlated with the degree of neurological dysfunction, suggesting acute injury as a potential underlying factor in this model. Treatment with CCX reduced the severity of trauma, alleviating both seizure activity and neurological dysfunction.

MRI has been widely used to detect abnormal brain conditions in vivo, providing a direct quantification of the damaged area (Mendoza et al. 2019). Our results indicated that the injury area progressively developed and expanded following a single $FeCl_2$ injection, suggesting that damage continues to progress under the influence of various pathological factors (Magid-Bernstein et al. 2022). Treatment with CCX significantly reduced the injury area and inhibited the spread of damage, effectively alleviating tissue damage caused by $FeCl_2$ injection. Observations of stained tissue sections (*i.e.*, H&E, Nissl, Golgi, and Perls) further confirmed that CCX exerts neuroprotective effects by inhibiting cell damage, cell loss, synaptic changes, and the deposition of iron-containing heme.

The widespread activation, proliferation, and recruitment of glial cells play critical roles in the development of post-traumatic epilepsy (Bedner et al. 2015; Eyo et al. 2017). Glial scar formation has been recognized as a hallmark of

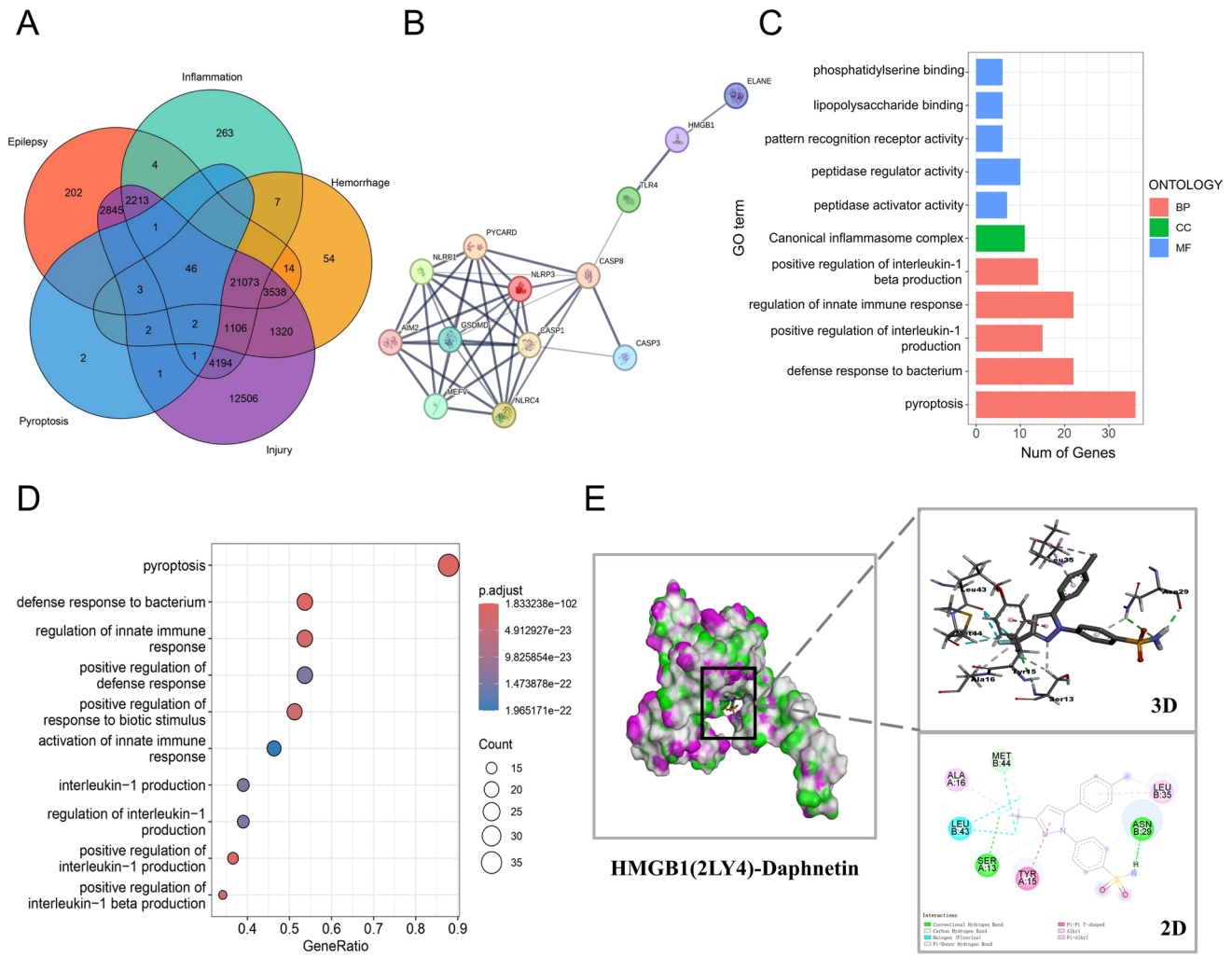

Fig. 9 GO functional enrichment analysis. **A** Venn diagram of selected genes. **B** PPI network. **C–D** GO enrichment analysis. **E** Molecular docking of CCX and HMGB1

chronic focal epilepsy (Eid et al. 2019; Wu et al. 2020). Following massive intracerebral hemorrhage, primary and secondary injuries stimulate neurons to rapidly release HMGB1, which activates TLRs on neuronal and glial cell membranes (Famakin et al. 2020; Waltl et al. 2018). In response, activated glial cells migrate to the injury site, where they trigger an inflammatory cascade that lowers the seizure threshold (Fig. 11). IF staining confirmed that $FeCl_2$ injection triggered the activation and recruitment of microglia to the injured cortex. Interestingly, despite no direct damage to the hippocampus, microglia in this region displayed significant activation and a tendency to migrate toward the frontal cortex. This result suggests that signals from the injured cortex can induce hippocampal microglial recruitment for phagocytosis. In addition to microglial migration, extensive astrocyte proliferation was observed in the CA1, CA3, and DG regions of the hippocampus. Epileptogenic foci in acquired epilepsy can originate from different locations, and glial cell proliferation is common across various epilepsy types (Leite and Peixoto-Santos 2021). Our data indicate that following $FeCl_2$ injection, seizures might expand beyond the injury site to involve hippocampal glial proliferation. During the early stages of traumatic hemorrhage, modulating glial cell behavior might thus represent a potential therapeutic target for different types of epilepsy (Leite and Peixoto-Santos 2021). In addition to inhibiting microglial polarization and reducing their recruitment to the injury site, CCX treatment mitigated astrocyte proliferation in the hippocampus, potentially preventing the formation of epileptogenic foci. These findings provide insights into the mechanisms of temporal lobe epilepsy induced by brain trauma.

Cell death and lysis in the injury area are key contributors to inflammation (Tang et al. 2019; Wen et al. 2019). Li et al. reported that baicalein inhibited iron-induced cell death and alleviated post-traumatic seizures (Li et al. 2019). In our study, we found that cells in the frontal cortex were

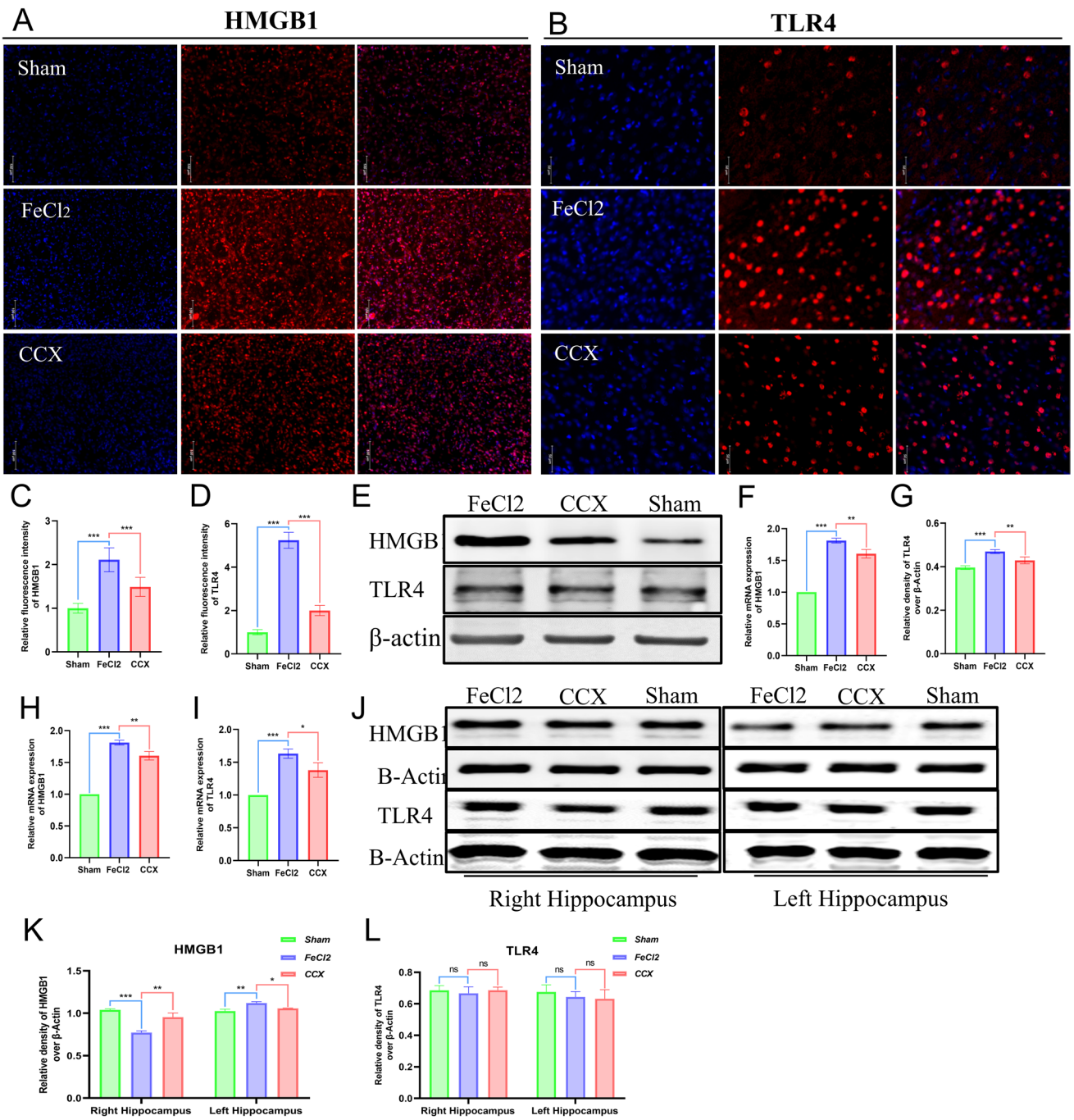

Fig. 10 CCX modulates inflammation and the HMGB1/TLR4 axis. **A–B** IF staining images of HMGB1/TLR4 in the frontal cortex at 7 days post-surgery. **C–D** Fluorescence intensity of HMGB1 and TLR4. **E** WB of HMGB1 and TLR4 in the frontal cortex at 7 days post-surgery. **F–G** Relative protein expression of HMGB1 and TLR4. **H–I** Relative mRNA expression of HMGB1 and TLR4 in the frontal cortex at 7 days post-surgery. **J** WB of HMGB1 and TLR4 in bilateral hippocampi at 7 days post-surgery. **K–L** Relative protein expression of HMGB1 and TLR4. ***$p < 0.001$, **$p < 0.01$, *$p < 0.05$

damaged following $FeCl_2$ injection, leading to programmed death. However, there was no significant upregulation of inflammatory factors at 24 h post-injection. Ferroptosis is known to occur immediately after ICH (Sun et al. 2022). At 7 days post-injection, a significant increase in inflammatory factor levels was observed, indicating the onset of inflammation. These findings imply that lytic cells release signals that activate and recruit microglia to clear cellular debris and that microglial activation further amplifies inflammation through the secretion of signaling factors (Wang et al. 2020). TUNEL

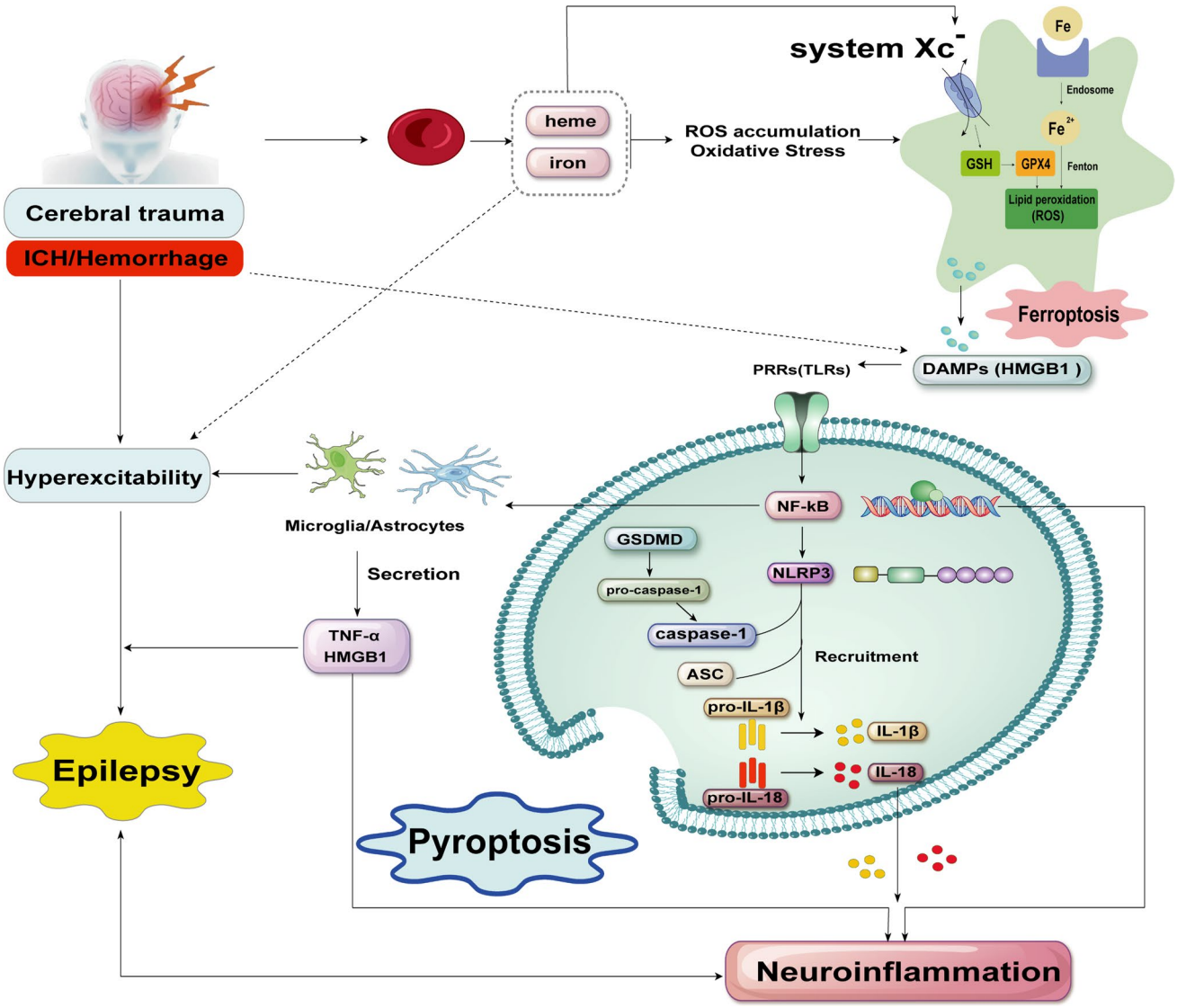

Fig. 11 Crosstalk among glial cells, pyroptosis, ferroptosis, and the HMGB1/TLR4 axis

staining revealed significant cell death in the cortex following $FeCl_2$ injection, which was alleviated by CCX treatment through the inhibition of inflammation. Further TEM analysis detected pyroptotic bodies and shortened mitochondria, which are key characteristics of pyroptosis and ferroptosis, respectively (Li et al. 2020; Shi et al. 2017). Other analyses confirmed the activation of the caspase-1–mediated classical pyroptotic pathway and the depletion of GPX4 and xCT in the $FeCl_2$-induced seizure model. Collectively, we concluded that after $FeCl_2$ injection, multiple forms of cell death occur, and the anti-inflammatory and protective effects of CCX are primarily mediated through the inhibition of pyroptosis. Notably, the significantly increased recruitment and proliferation of astrocytes in the hippocampus were similar to that observed in the frontal cortex following $FeCl_2$ injection, implying the occurrence of similar inflammatory processes in the hippocampus. However, we did not observe significant cell death or upregulation of inflammatory factors in the hippocampus, contradicting findings reported in chronic epilepsy models (Irrera et al. 2020; Nathalie et al. 2021; Sun et al. 2020). The discrepancy might be attributable to distinct inflammatory mechanisms in the hippocampus relative to the frontal cortex during the early stages of injury (Magid-Bernstein et al. 2022). It can also be speculated that late-onset epileptic seizures or temporal lobe epilepsy are not driven by inflammation alone.

The HMGB1/TLR4 axis, functioning as both a chemotactic pathway and pro-inflammatory mediator, activates pyroptosis, induces tissue damage (Sun et al. 2020; Tang et al. 2023), and promotes the transcription and expression of inflammasomes (Fig. 11). Previous molecular docking studies found that multiple compounds can directly bind

to HMGB1 (Alzokaky et al. 2023; Gao et al. 2022; Tripathi et al. 2019). Our results revealed that CCX exerts its pharmacological effects by directly binding to HMGB1. We further confirmed that CCX significantly suppresses the HMGB1/TLR4 axis in the frontal cortex in $FeCl_2$-injected rats. These results support that CCX reduces pyroptosis and inflammation by inhibiting the HMGB1/TLR4 axis. Interestingly, we also observed an asymmetric pattern of HMGB1 expression in the hippocampus. Based on the finding that HMGB1 is involved in the migration of hippocampal microglia (Chen et al. 2022b; Wang et al. 2020), we speculated that this asymmetric pattern is related to microglial migration from the hippocampus to the frontal cortex. The significant microglial migration from the ipsilateral hippocampus leads to a decrease in HMGB1 expression, whereas on the contralateral side, the proliferation of astrocytes induces the upregulation of HMGB1 despite minimal microglial migration. This finding further suggests that the inflammatory mechanisms in the hippocampus differ from those in the frontal cortex in this model. These findings suggest that HMGB1 both participates in $FeCl_2$-induced epilepsy by regulating inflammation and influences the onset and progression of epilepsy by modulating glial cell behavior. CCX, by inhibiting the HMGB1/TLR4 axis, alleviates cell pyroptosis and glial cell activation and proliferation, ultimately inhibiting inflammation and exerting protective and ante-epileptic effects.

Although the results of our study are promising, several limitations should be acknowledged. First, continuous monitoring of rat seizures using electroencephalograms was not performed because of equipment constraints. Second, the specificity of HMGB1 agonists and inhibitors in rats remains suboptimal, preventing a further investigation of the relationship between the HMGB1/TLR4 axis and pyroptosis. To address these limitations, future studies will involve cell culture experiments and the construction of a pyroptosis model, in which the expression of HMGB1 will be controlled via plasmid transfection. Furthermore, the abnormal reduction of HMGB1 expression in the ipsilateral hippocampus, accompanied by microglial migration to the cortex, warrants further exploration to determine whether hippocampal HMGB1 is primarily secreted by microglia. Third, future work should include co-localization analyses of pyroptosis markers with cell type-specific markers (NeuN, Iba1, GFAP) to identify the predominant cell populations undergoing pyroptosis. Lastly, the classical NF-κB activation pathway involves degradation of IκB and nuclear translocation of its subunit p65/RelA, and these processes are essential for transcriptional regulation. In this study, we did not directly assess p65 localization, and further experiments (e.g., WB) are required to validate NF-κB activation. Additionally, inflammasome activation causes ASC to form large, insoluble oligomers, detectable as high-molecular weight bands on WB. Our study did not evaluate ASC oligomerization, and future experiments are needed to confirm these molecular changes in addition to the soluble monomer band.

Conclusions

Our study demonstrated that the HMGB1/TLR4 pathway plays an important role in $FeCl_2$-induced epilepsy in rats. CCX mitigates the severity of epilepsy and associated injury by suppressing this axis. These findings suggest that during the early stages of injury, ferroptotic cells release HMGB1, which activates microglia and induces inflammation, leading to pyroptosis. CCX inhibits this process by downregulating HMGB1, thereby inhibiting pyroptosis and alleviating the severity of injury and seizures.

Supplementary Information The online version contains supplementary material available at https://doi.org/10.1007/s10571-025-01615-4.

Acknowledgements This work was supported by the Ningxia Key Laboratory of Cerebrocranial Disease, which provided valuable assistance with the laboratory and field tests.

Author Contributions Yu Sun, Feng Wang, and Weifang Rong wrote the manuscript and participated in all aspects of the experimental design and research procedure. Shucai Jiang participated in the operation and analysis of all epilepsy and behavioral measurements. Lei Chen and Yan Feng helped with the MRI and electroencephalography data. Zhe Feng participated in the sample preparation and molecular biology experiments. Caibin Gao was involved in the design of the study and interpretation of the figures and manuscript. All authors have read and approved the final manuscript.

Funding The National Natural Science Foundation of China (NSFC, No. 82060261) supported this study.

Data Availability The datasets generated and analyzed during the current study are available from the corresponding author on reasonable request.

Declarations

Conflict of Interests The authors declare that they have no conflict of interest.

Ethical Approval All animal experiments complied with the ARRIVE guidelines, and the procedures were performed in accordance with the Laboratory Animal Ethics and Welfare Committee of Ningxia Medical University's Laboratory Animal Center (Ethical Review of Scientific Research No. 2019152).

Consent to Participate Not applicable.

Consent to Publish Not applicable.

Clinical Trial Number Not applicable.

References

Alzokaky AA, Al-Karmalawy AA, Saleh MA, Abdo W, Farage AE, Belal A, Abourehab MAS, Antar SA (2023) Metformin ameliorates doxorubicin-induced cardiotoxicity targeting HMGB1/TLR4/NLRP3 signaling pathway in mice. Life Sci 316:121390. https://doi.org/10.1016/j.lfs.2023.121390

Andersson U, Yang H, Harris H (2018a) Extracellular HMGB1 as a therapeutic target in inflammatory diseases. Expert Opin Ther Targets 22:263–277. https://doi.org/10.1080/14728222.2018.1439924

Andersson U, Yang H, Harris H (2018b) High-mobility group box 1 protein (HMGB1) operates as an alarmin outside as well as inside cells. Semin Immunol 38:40–48. https://doi.org/10.1016/j.smim.2018.02.011

Atabaki R, Khaleghzadeh-Ahangar H, Esmaeili N, Mohseni-Moghaddam P (2023) Role of pyroptosis, a pro-inflammatory programmed cell death, in epilepsy. Cell Mol Neurobiol 43:1049–1059. https://doi.org/10.1007/s10571-022-01250-3

Banks WA, Hansen KM, Erickson MA, Crews FT (2023) High-mobility group box 1 (HMGB1) crosses the BBB bidirectionally. Brain Behav Immun 111:386–394. https://doi.org/10.1016/j.bbi.2023.04.018

Bedner P, Dupper A, Hüttmann K et al (2015) Astrocyte uncoupling as a cause of human temporal lobe epilepsy. Brain 138:1208–1222. https://doi.org/10.1093/brain/awv067

Burdette BE, Esparza AN, Zhu H, Wang S (2021) Gasdermin d in pyroptosis. Acta Pharm Sin B 11:2768–2782. https://doi.org/10.1016/j.apsb.2021.02.006

Caliaperumal J, Ma Y, Colbourne F (2012) Intra-parenchymal ferrous iron infusion causes neuronal atrophy, cell death and progressive tissue loss: implications for intracerebral hemorrhage. Exp Neurol 237:363–369. https://doi.org/10.1016/j.expneurol.2012.07.001

Chen X, Kang R, Kroemer G, Tang D (2021) Ferroptosis in infection, inflammation, and immunity. J Exp Med. https://doi.org/10.1084/jem.20210518

Chen KN, Guan QW, Yin XX, Wang ZJ, Zhou HH, Mao XY (2022a) Ferrostatin-1 obviates seizures and associated cognitive deficits in ferric chloride-induced posttraumatic epilepsy via suppressing ferroptosis. Free Radic Biol Med 179:109–118. https://doi.org/10.1016/j.freeradbiomed.2021.12.268

Chen R, Kang R, Tang D (2022b) The mechanism of HMGB1 secretion and release. Exp Mol Med 54:91–102. https://doi.org/10.1038/s12276-022-00736-w

Conrad M, Lorenz SM, Proneth B (2021) Targeting ferroptosis: new hope for as-yet-incurable diseases. Trends Mol Med 27:113–122. https://doi.org/10.1016/j.molmed.2020.08.010

Corps KN, Roth TL, McGavern DB (2015) Inflammation and neuroprotection in traumatic brain injury. JAMA Neurol 72:355–362. https://doi.org/10.1001/jamaneurol.2014.3558

Das J, Singh R, Sharma D (2017) Antiepileptic effect of fisetin in iron-induced experimental model of traumatic epilepsy in rats in the light of electrophysiological, biochemical, and behavioral observations. Nutr Neurosci 20:255–264. https://doi.org/10.1080/1028415x.2016.1183342

Dedeurwaerdere S, Friedman A, Fabene PF, Mazarati A, Murashima YL, Vezzani A, Baram TZ (2012) Finding a better drug for epilepsy: antiinflammatory targets. Epilepsia 53:1113–1118. https://doi.org/10.1111/j.1528-1167.2012.03520.x

Eid T, Lee TW, Patrylo P, Zaveri HP (2019) Astrocytes and glutamine synthetase in epileptogenesis. J Neurosci Res 97:1345–1362. https://doi.org/10.1002/jnr.24267

Eyo UB, Murugan M, Wu LJ (2017) Microglia-neuron communication in epilepsy. Glia 65:5–18. https://doi.org/10.1002/glia.23006

Famakin BM, Tsymbalyuk O, Tsymbalyuk N, Ivanova S, Woo SK, Kwon MS, Gerzanich V, Simard JM (2020) HMGB1 is a potential mediator of astrocytic TLR4 signaling activation following acute and chronic focal cerebral ischemia. Neurol Res Int 2020:3929438. https://doi.org/10.1155/2020/3929438

Fong CY, Tay CG, Ong LC, Lai NM (2017) Chloral hydrate as a sedating agent for neurodiagnostic procedures in children. Cochrane Database Syst Rev. https://doi.org/10.1002/14651858.CD011786.pub2

Frank D, Vince JE (2019) Pyroptosis versus necroptosis: similarities, differences, and crosstalk. Cell Death Differ 26:99–114. https://doi.org/10.1038/s41418-018-0212-6

Gao JM, Zhang X, Shu GT et al (2022) Trilobatin rescues cognitive impairment of Alzheimer's disease by targeting HMGB1 through mediating SIRT3/SOD2 signaling pathway. Acta Pharmacol Sin 43:2482–2494. https://doi.org/10.1038/s41401-022-00888-5

Hirano T, Enatsu R, Iihoshi S, Mikami T, Honma T, Ohnishi H, Mikuni N (2019) Effects of hemosiderosis on epilepsy following subarachnoid hemorrhage. Neurol Med Chir (Tokyo) 59:27–32. https://doi.org/10.2176/nmc.oa.2018-0125

Hsu SK, Li CY, Lin IL, Syue WJ, Chen YF, Cheng KC, Teng YN, Lin YH, Yen CH, Chiu CC (2021) Inflammation-related pyroptosis, a novel programmed cell death pathway, and its crosstalk with immune therapy in cancer treatment. Theranostics 11:8813–8835. https://doi.org/10.7150/thno.62521

Huang Y, Zhang X, Huang Q, Dou Y, Qu C, Xu Q, Yuan Q, Xian YF, Lin ZX (2022) Quercetin enhances survival and axonal regeneration of motoneurons after spinal root avulsion and reimplantation: experiments in a rat model of brachial plexus avulsion. Inflamm Regen 42:56. https://doi.org/10.1186/s41232-022-00245-3

Irrera N, Russo M, Pallio G, Bitto A, Mannino F, Minutoli L, Altavilla D, Squadrito F (2020) The role of NLRP3 inflammasome in the pathogenesis of traumatic brain injury. Int J Mol Sci. https://doi.org/10.3390/ijms21176204

Jiang X, Stockwell BR, Conrad M (2021) Ferroptosis: mechanisms, biology and role in disease. Nat Rev Mol Cell Biol 22:266–282. https://doi.org/10.1038/s41580-020-00324-8

Kamaşak T, Dilber B, Yaman S, Durgut BD, Kurt T, Çoban E, Arslan EA, Şahin S, Karahan SC, Cansu A (2020) HMGB-1, TLR4, IL-1R1, TNF-α, and IL-1β: novel epilepsy markers? Epileptic Disord 22:183–193. https://doi.org/10.1684/epd.2020.1155

Keith KA, Huang JH (2019) Animal models of post-traumatic epilepsy. Diagnostics. https://doi.org/10.3390/diagnostics10010004

Komatsu M, Hiramatsu M, Willmore LJ (2000) Zonisamide reduces the increase in 8-hydroxy-2'-deoxyguanosine levels formed during iron-induced epileptogenesis in the brains of rats. Epilepsia 41:1091–1094. https://doi.org/10.1111/j.1528-1157.2000.tb00312.x

Leite JP, Peixoto-Santos JE (2021) Glia and extracellular matrix molecules: what are their importance for the electrographic and MRI changes in the epileptogenic zone? Epilepsy Behav 121:106542. https://doi.org/10.1016/j.yebeh.2019.106542

Li Q, Li QQ, Jia JN, Sun QY, Zhou HH, Jin WL, Mao XY (2019) Baicalein exerts neuroprotective effects in FeCl(3)-induced

posttraumatic epileptic seizures via suppressing ferroptosis. Front Pharmacol 10:638. https://doi.org/10.3389/fphar.2019.00638
Li J, Cao F, Yin HL, Huang ZJ, Lin ZT, Mao N, Sun B, Wang G (2020) Ferroptosis: past, present and future. Cell Death Dis 11:88. https://doi.org/10.1038/s41419-020-2298-2
Loveless R, Bloomquist R, Teng Y (2021) Pyroptosis at the forefront of anticancer immunity. J Exp Clin Cancer Res 40:264. https://doi.org/10.1186/s13046-021-02065-8
Lüttjohann A, Fabene PF, van Luijtelaar G (2009) A revised Racine's scale for PTZ-induced seizures in rats. Physiol Behav 98:579–586. https://doi.org/10.1016/j.physbeh.2009.09.005
Maas AI, Stocchetti N, Bullock R (2008) Moderate and severe traumatic brain injury in adults. Lancet Neurol 7:728–741. https://doi.org/10.1016/s1474-4422(08)70164-9
Magid-Bernstein J, Girard R, Polster S, Srinath A, Romanos S, Awad IA, Sansing LH (2022) Cerebral hemorrhage: pathophysiology, treatment, and future directions. Circ Res 130:1204–1229. https://doi.org/10.1161/circresaha.121.319949
Mendoza K, Derry PJ, Cherian LM, Garcia R, Nilewski L, Goodman JC, Mbye L, Robertson CS, Tour JM, Kent TA (2019) Functional and structural improvement with a catalytic carbon nano-antioxidant in experimental traumatic brain injury complicated by hypotension and resuscitation. J Neurotrauma 36:2139–2146. https://doi.org/10.1089/neu.2018.6027
Morgan A, Gaulden A, Altemus M, Williford K, Centanni S, Winder D, Patel S (2020) Cyclooxygenase-2 inhibition prevents stress induced amygdala activation and anxiety-like behavior. Brain Behav Immun 89:513–517. https://doi.org/10.1016/j.bbi.2020.07.046
Nathalie M, Polineni SP, Chin CN et al (2021) Targeting microglial polarization to improve TBI outcomes. CNS Neurol Disord Drug Targets 20:216–227. https://doi.org/10.2174/1871527319666200918145903
Paudel YN, Semple BD, Jones NC, Othman I, Shaikh MF (2019) High mobility group box 1 (HMGB1) as a novel frontier in epileptogenesis: from pathogenesis to therapeutic approaches. J Neurochem 151:542–557. https://doi.org/10.1111/jnc.14663
Ping X, Chai Z, Wang W, Ma C, White FA, Jin X (2021) Blocking receptor for advanced glycation end products (RAGE) or toll-like receptor 4 (TLR4) prevents posttraumatic epileptogenesis in mice. Epilepsia 62:3105–3116. https://doi.org/10.1111/epi.17069
Prakash C, Mishra M, Kumar P, Kumar V, Sharma D (2019) Dehydroepiandrosterone alleviates oxidative stress and apoptosis in iron-induced epilepsy via activation of Nrf2/ARE signal pathway. Brain Res Bull 153:181–190. https://doi.org/10.1016/j.brainresbull.2019.08.019
Prakash C, Mishra M, Kumar P, Kumar V, Sharma D (2021) Response of voltage-gated sodium and calcium channels subtypes on dehydroepiandrosterone treatment in iron-induced epilepsy. Cell Mol Neurobiol 41:279–292. https://doi.org/10.1007/s10571-020-00851-0
Puljak L, Marin A, Vrdoljak D, Markotic F, Utrobicic A, Tugwell P (2017) Celecoxib for osteoarthritis. Cochrane Database Syst Rev 5:Cd009865. https://doi.org/10.1002/14651858.CD009865.pub2
Qureshi AI, Mendelow AD, Hanley DF (2009) Intracerebral haemorrhage. Lancet 373:1632–1644. https://doi.org/10.1016/s0140-6736(09)60371-8
Ravizza T, Terrone G, Salamone A, Frigerio F, Balosso S, Antoine DJ, Vezzani A (2018) High mobility group box 1 is a novel pathogenic factor and a mechanistic biomarker for epilepsy. Brain Behav Immun 72:14–21. https://doi.org/10.1016/j.bbi.2017.10.008
Rawat C, Kukal S, Dahiya UR, Kukreti R (2019) Cyclooxygenase-2 (COX-2) inhibitors: future therapeutic strategies for epilepsy management. J Neuroinflammation 16:197. https://doi.org/10.1186/s12974-019-1592-3
Shi J, Gao W, Shao F (2017) Pyroptosis: gasdermin-mediated programmed necrotic cell death. Trends Biochem Sci 42:245–254. https://doi.org/10.1016/j.tibs.2016.10.004
Sun Z, Nyanzu M, Yang S et al (2020) VX765 attenuates pyroptosis and HMGB1/TLR4/NF-κB pathways to improve functional outcomes in TBI mice. Oxid Med Cell Longev 2020:7879629. https://doi.org/10.1155/2020/7879629
Sun Y, Li Q, Guo H, He Q (2022) Ferroptosis and iron metabolism after intracerebral hemorrhage. Cells. https://doi.org/10.3390/cells12010090
Tanaka T, Fukuma K, Abe S et al (2023) Association of cortical superficial siderosis with post-stroke epilepsy. Ann Neurol 93:357–370. https://doi.org/10.1002/ana.26497
Tang D, Kang R, Berghe TV, Vandenabeele P, Kroemer G (2019) The molecular machinery of regulated cell death. Cell Res 29:347–364. https://doi.org/10.1038/s41422-019-0164-5
Tang D, Kang R, Zeh HJ, Lotze MT (2023) The multifunctional protein HMGB1: 50 years of discovery. Nat Rev Immunol 23:824–841. https://doi.org/10.1038/s41577-023-00894-6
Thijs RD, Surges R, O'Brien TJ, Sander JW (2019) Epilepsy in adults. Lancet 393:689–701. https://doi.org/10.1016/s0140-6736(18)32596-0
Tian Y, Cao Y, Chen R, Jing Y, Xia L, Zhang S, Xu H, Su Z (2020) HMGB1 a box protects neurons by potently inhibiting both microglia and T cell-mediated inflammation in a mouse Parkinson's disease model. Clin Sci 134:2075–2090. https://doi.org/10.1042/cs20200553
Tripathi A, Shrinet K, Singh VK, Kumar A (2019) Molecular modelling and docking of *Mus musculus* HMGB1 inflammatory protein with CGA. Bioinformation 15:467–473. https://doi.org/10.6026/97320630015467
van Vliet EA, Aronica E, Vezzani A, Ravizza T (2018) Neuroinflammatory pathways as treatment targets and biomarker candidates in epilepsy: emerging evidence from preclinical and clinical studies. Neuropathol Appl Neurobiol 44:91–111. https://doi.org/10.1111/nan.12444
Vezzani A, Balosso S, Ravizza T (2008) The role of cytokines in the pathophysiology of epilepsy. Brain Behav Immun 22:797–803. https://doi.org/10.1016/j.bbi.2008.03.009
Vezzani A, French J, Bartfai T, Baram TZ (2011) The role of inflammation in epilepsy. Nat Rev Neurol 7:31–40. https://doi.org/10.1038/nrneurol.2010.178
Waltl I, Käufer C, Gerhauser I, Chhatbar C, Ghita L, Kalinke U, Löscher W (2018) Microglia have a protective role in viral encephalitis-induced seizure development and hippocampal damage. Brain Behav Immun 74:186–204. https://doi.org/10.1016/j.bbi.2018.09.006
Wang B, Huang X, Pan X, Zhang T, Hou C, Su WJ, Liu LL, Li JM, Wang YX (2020) Minocycline prevents the depressive-like behavior through inhibiting the release of HMGB1 from microglia and neurons. Brain Behav Immun 88:132–143. https://doi.org/10.1016/j.bbi.2020.06.019
Wen Q, Liu J, Kang R, Zhou B, Tang D (2019) The release and activity of HMGB1 in ferroptosis. Biochem Biophys Res Commun 510:278–283. https://doi.org/10.1016/j.bbrc.2019.01.090
Willmore LJ, Rubin JJ (1982) Formation of malonaldehyde and focal brain edema induced by subpial injection of FeCl2 into rat isocortex. Brain Res 246:113–119. https://doi.org/10.1016/0006-8993(82)90147-0
Willmore LJ, Sypert GW, Munson JB (1978a) Recurrent seizures induced by cortical iron injection: a model of posttraumatic epilepsy. Ann Neurol 4:329–336. https://doi.org/10.1002/ana.410040408
Willmore LJ, Sypert GW, Munson JV, Hurd RW (1978b) Chronic focal epileptiform discharges induced by injection of iron into rat and

cat cortex. Science 200:1501–1503. https://doi.org/10.1126/science.96527

Wu F, Xu K, Liu L et al (2019) Vitamin b(12) enhances nerve repair and improves functional recovery after traumatic brain injury by inhibiting ER stress-induced neuron injury. Front Pharmacol 10:406. https://doi.org/10.3389/fphar.2019.00406

Wu W, Li Y, Wei Y, Bosco DB, Xie M, Zhao MG, Richardson JR, Wu LJ (2020) Microglial depletion aggravates the severity of acute and chronic seizures in mice. Brain Behav Immun 89:245–255. https://doi.org/10.1016/j.bbi.2020.06.028

Yan HF, Zou T, Tuo QZ, Xu S, Li H, Belaidi AA, Lei P (2021) Ferroptosis: mechanisms and links with diseases. Signal Transduct Target Ther 6:49. https://doi.org/10.1038/s41392-020-00428-9

Yang W, Li J, Shang Y, Zhao L, Wang M, Shi J, Li S (2017) HMGB1-TLR4 axis plays a regulatory role in the pathogenesis of mesial temporal lobe epilepsy in immature rat model and children via the p38MAPK signaling pathway. Neurochem Res 42:1179–1190. https://doi.org/10.1007/s11064-016-2153-0

Zhou L, Zhou L, Su LD et al (2018) Celecoxib ameliorates seizure susceptibility in autosomal dominant lateral temporal epilepsy. J Neurosci 38:3346–3357. https://doi.org/10.1523/jneurosci.3245-17.2018